5-2018

Downregulation of MicroRNA Eca-Mir-128 in Seminal Exosomes and Enhanced Expression of CXCL16 in the Stallion Reproductive Tract Are Associated with Long-Term Persistence of Equine Arteritis Virus

Mariano Carossino
University of Kentucky, mcarossino@uky.edu

Pouya Dini
University of Kentucky, pouya.dini@uky.edu

Theodore S. Kalbfleisch
University of Louisville

Alan T. Loynachan
University of Kentucky, alan.loynachan@uky.edu

Igor F. Canisso
University of Illinois at Urbana-Champaign

Authors

Mariano Carossino, Pouya Dini, Theodore S. Kalbfleisch, Alan T. Loynachan, Igor F. Canisso, Kathleen M. Shuck, Peter J. Timoney, R. Frank Cook, and Udeni B. R. Balasuriya

Downregulation of MicroRNA Eca-Mir-128 in Seminal Exosomes and Enhanced Expression of CXCL16 in the Stallion Reproductive Tract Are Associated with Long-Term Persistence of Equine Arteritis Virus

Downregulation of MicroRNA eca-mir-128 in Seminal Exosomes and Enhanced Expression of CXCL16 in the Stallion Reproductive Tract Are Associated with Long-Term Persistence of Equine Arteritis Virus

Mariano Carossino,[a] Pouya Dini,[a,b] Theodore S. Kalbfleisch,[c] Alan T. Loynachan,[d] Igor F. Canisso,[e,f] Kathleen M. Shuck,[a] Peter J. Timoney,[a] R. Frank Cook,[a] Udeni B. R. Balasuriya[a]

[a]Maxwell H. Gluck Equine Research Center, Department of Veterinary Science, University of Kentucky, Lexington, Kentucky, USA

[b]Department of Veterinary Imaging, Faculty of Veterinary Medicine, Ghent University, Merelbeke, Belgium

[c]Department of Biochemistry and Molecular Genetics, School of Medicine, University of Louisville, Louisville, Kentucky, USA

[d]University of Kentucky Veterinary Diagnostic Laboratory, Department of Veterinary Science, University of Kentucky, Lexington, Kentucky, USA

[e]Department of Veterinary Clinical Medicine, College of Veterinary Medicine, University of Illinois Urbana-Champaign, Urbana, Illinois, USA

[f]Department of Comparative Biosciences, College of Veterinary Medicine, University of Illinois Urbana-Champaign, Urbana, Illinois, USA

ABSTRACT Equine arteritis virus (EAV) can establish long-term persistent infection in the reproductive tract of stallions and is shed in the semen. Previous studies showed that long-term persistence is associated with a specific allele of the *CXCL16* gene (*CXCL16S*) and that persistent infection is maintained despite the presence of a local inflammatory and humoral and mucosal antibody responses. In this study, we demonstrated that equine seminal exosomes (SEs) are enriched in a small subset of microRNAs (miRNAs). Most importantly, we demonstrated that long-term EAV persistence is associated with the downregulation of an SE-associated miRNA (eca-mir-128) and with an enhanced expression of CXCL16 in the reproductive tract, a putative target of eca-mir-128. The findings presented here suggest that SE eca-mir-128 is implicated in the regulation of the CXCL16/CXCR6 axis in the reproductive tract of persistently infected stallions, a chemokine axis strongly implicated in EAV persistence. This is a novel finding and warrants further investigation to identify its specific mechanism in modulating the CXCL16/CXCR6 axis in the reproductive tract of the EAV long-term carrier stallion.

IMPORTANCE Equine arteritis virus (EAV) has the ability to establish long-term persistent infection in the stallion reproductive tract and to be shed in semen, which jeopardizes its worldwide control. Currently, the molecular mechanisms of viral persistence are being unraveled, and these are essential for the development of effective therapeutics to eliminate persistent infection. Recently, it has been determined that long-term persistence is associated with a specific allele of the *CXCL16* gene (*CXCL16S*) and is maintained despite induction of local inflammatory, humoral, and mucosal antibody responses. This study demonstrated that long-term persistence is associated with the downregulation of seminal exosome miRNA eca-mir-128 and enhanced expression of its putative target, CXCL16, in the reproductive tract. For the first time, this study suggests complex interactions between eca-mir-128 and cellular elements at the site of EAV persistence and implicates this miRNA in the regulation of the CXCL16/CXCR6 axis in the reproductive tract during long-term persistence.

Equine viral arteritis (EVA) is an economically important systemic, reproductive, and respiratory disease of equids (1–7, 12). Its causative agent, equine arteritis virus (EAV), is a positive-sense, single-stranded RNA virus that belongs to the family *Arteriviridae*, order *Nidovirales* (8). This virus can be readily transmitted via the respiratory or venereal routes by the acutely infected horse or solely through the venereal route by the carrier stallion (3, 7, 9–11). Viral infection can be either asymptomatic or associated with a wide range of clinical signs (influenza-like syndrome), including dependent edema, conjunctivitis, periorbital or supraorbital edema, respiratory distress, urticaria, and leukopenia (1–3, 7, 12–19). Additionally, EAV infection of pregnant mares can result in abortion or birth of congenitally infected foals that develop a rapidly progressive and ultimately fatal bronchointerstitial pneumonia or pneumoenteric syndrome (20). Very importantly, EAV can establish persistent infection in the reproductive tract of stallions (carrier state), resulting in continuous shedding of infectious virus in their semen (1–3, 26), which guarantees perpetuation of the virus in equine populations (1–3, 6, 7, 9–12, 21–24). The carrier state is testosterone dependent (25) and can last from several weeks or months (i.e., virus shedding in semen ≤1 year following infection [short-term carrier]) to years or even lifelong (i.e., virus shedding in semen >1 year following infection [long-term carrier]) in spite of the development of strong serum neutralizing antibody, mucosal antibody, and local inflammatory responses in the reproductive tract (3, 7, 9, 11, 21, 23, 26–28). Interestingly, EAV carrier stallions do not exhibit clinical signs of disease and exhibit no impairment of fertility (7, 11, 19, 23). To date, the immunopathogenesis of persistent EAV infection in the reproductive tract of the stallion is not completely understood, and it is under investigation in our laboratory. Recently, it has been shown that the outcome of EAV infection in the stallion is dependent on host genetic factors (28–31), precisely associated with a specific allele of the *CXCL16* gene (*CXCL16S*), and that EAV has a specific tropism for a subset of T and B lymphocytes and stromal cells primarily in the ampullae and, to a lesser extent, in the other accessory sex glands (vesicular, prostate, and bulbourethral glands) of the persistently infected stallion (26). Moreover, EAV can persist in the male genital tract despite the presence of strong inflammatory (mediated mainly by CD8$^+$ T lymphocytes) and EAV-specific mucosal antibody responses (26, 27). It is paramount to better understand the mechanisms of EAV persistent infection in the stallion reproductive tract in order to enable development of novel therapies for elimination of the carrier state.

Semen is a complex body fluid composed of cells (mainly spermatozoa and a smaller number of white blood cells) and seminal plasma (32–34). Seminal plasma components in equine semen, as well as in that of other species, have been previously characterized (35–40). Interestingly, in addition to the described soluble constituents, equine seminal plasma contains a diversity of extracellular vesicles, including seminal exosomes (SEs) (34, 41–46). Seminal exosomes encompass a broad group of exosomes, including prostasomes secreted by the prostatic epithelium as well as exosomes derived from other cell types within the reproductive tract (34, 41). Exosomes (including SEs) are derived from multivesicular bodies (MVBs), as opposed to microvesicles, which originate from the process of exocytosis (47). Currently, the properties and function of specific-cell derived exosomes are under extensive investigation. Previous studies have demonstrated that extracellular vesicles are immunosuppressive components in semen and are responsible for mediating the induction of tolerance to paternal antigens (34, 48, 49). Also, they have been implicated in the inhibition of lymphoproliferative responses, phagocytic activity, and natural killer (NK) cell functionality (34, 42). In addition, there is evidence that seminal plasma components may influence viral transmission and replication by either facilitating or blocking it; this property may be dependent on specific viral infections (34, 43, 50). Seminal exosomes participate in cell-cell communication by specific cargo delivery, which may include proteins (e.g.,

cytokines and growth factors), specific lipids, and coding and small noncoding RNAs with potential regulatory functions, including microRNAs (miRNAs) (34, 51). MicroRNAs are noncoding RNA molecules approximately 22 to 24 nucleotides (nt) in length that participate in posttranscriptional regulation of gene expression through specific degradation of mRNA targets or the blockade of their translation (52). Currently, extensive studies have been undertaken to elucidate the role of specific miRNAs in diverse disease processes and their potential use as biomarkers (53–58). Recently, equine miRNAs in normal tissues have been investigated (59, 60), and exosomes and exosomal miRNAs derived from serum and ovarian follicular fluid in mares have been characterized (61–63). Even though SEs have been described for the horse and their role during sperm capacitation has been studied (46, 64), their RNA cargo and function remain to be characterized. Thus, we hypothesized that in light of their potential regulatory functions, SE-associated miRNA species could play a role in the molecular pathogenesis of EAV persistence in the reproductive tract and contribute to viral immune evasion mechanisms. The primary objective of this study was to characterize the equine SE-associated miRNAs and define their potential role during EAV long-term persistent infection in the reproductive tract. We demonstrated that equine SEs are enriched in miRNAs, with potential implications in immune-mediated pathways as observed in humans. Most importantly, we have identified specific downregulation in the relative expression of SE eca-mir-128 during long-term EAV persistent infection and enhanced expression of CXCL16, a chemokine strongly implicated in EAV long-term persistence (21, 29–31), in the ampullae. Interestingly, we have determined that *CXCL16* mRNA constitutes a putative target of eca-mir-128 and that consequently, this miRNA may play a critical role in the regulation of the CXCL16/CXCR6 chemokine axis in the reproductive tract of the stallion. This finding is novel and warrants further investigation to identify the specific mechanism whereby it modulates the CXCL16/CXCR6 axis in the reproductive tract of the EAV long-term carrier stallion.

RESULTS

Isolation and size characterization of equine seminal exosomes. The equine exosomes present in two equine seminal plasma samples were precipitated overnight and analyzed by transmission electron microscopy (TEM). TEM analysis demonstrated the presence of membrane-bound particles that were either isolated or in clusters. Size distribution analysis determined a mean vesicle size of 93.43 nm, with 80.8% of the precipitated exosomes having a size ranging from 21 to 120 nm, while <20% comprised larger vesicles (>120 nm) (Fig. 1A and B). The vast majority of the vesicles (67%) had a size ranging from 41 to 100 nm.

Characterization of equine seminal exosomes by Western immunoblotting and immunogold labeling. Exosome-specific markers were evaluated in SEs derived from naive ($n = 10$), short-term ($n = 5$), and long-term persistently infected ($n = 5$) stallions by Western immunoblotting with a panel of specific antibodies (Table 1). Specifically, SEs were characterized by the expression of the tetraspanin protein CD9 and heat shock protein 70 (HSP70) (Fig. 1C) and lack of expression of calreticulin, a calcium-binding protein resident of the endoplasmic reticulum (ER) (Fig. 1C). The expression of CD63 was variable (detected in only 2/20 SE fractions analyzed), while SEs did not express CD81, vimentin, or major histocompatibility complex class II (MHC-II) (Table 2). Furthermore, immunogold staining demonstrated that expression of CD9 is associated with the exosomal membrane (Fig. 1B [inset]). Taken together, these data unequivocally demonstrated successful isolation of SEs from equine seminal plasma and no specific differences in the SE marker expression profiles among naive, short-term, and long-term persistently infected stallions.

Seminal exosomes contain extracellular RNA cargo with a higher abundance of small RNA species. Total RNA was isolated from SEs (derived from semen samples described in Materials and Methods and which were subsequently used for quantitative real-time reverse transcription-PCR [RT-qPCR] analysis as described below [naive stallions, $n = 15$; short-term carrier stallions, $n = 7$; and long-term carrier stallions, $n = 18$]),
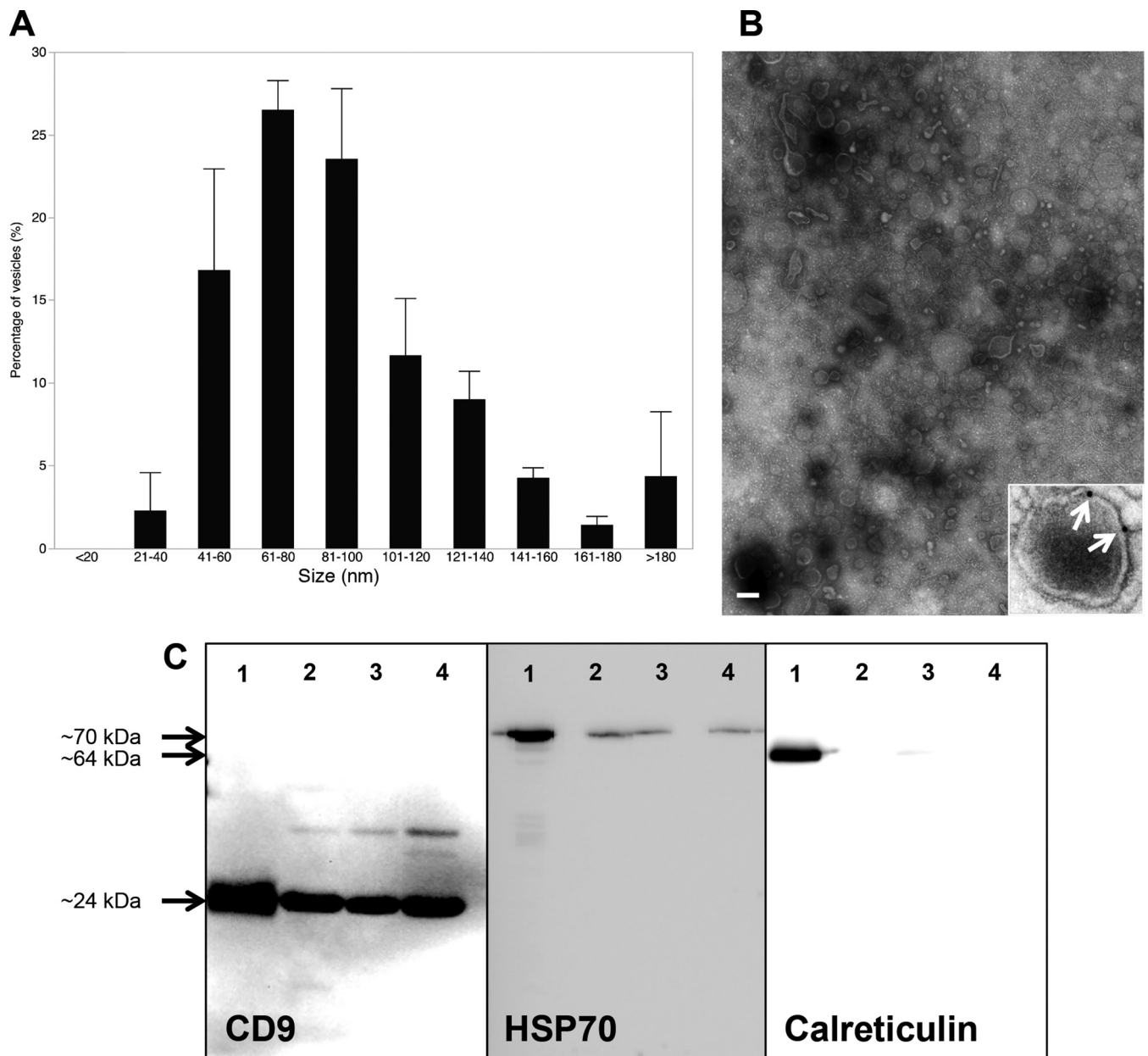
FIG 1 Isolation and characterization of equine seminal exosomes. (A) SEs had a mean diameter of 93.43 nm, with the vast majority having a size range between 21 and 120 nm. (B) TEM imaging of precipitated SEs. Filamentous structures in SE preparations were also present, as previously observed in the case of equine semen. Bar = 100 μm. (Inset) Note the localization of CD9 on the exosome membrane (arrows; immunogold labeling). (C) Characterization of isolated SEs by Western immunoblotting analysis. High expression of CD9 and HSP70 was observed in SEs derived from naive and short-term and long-term EAV carrier stallions (lanes 2, 3, and 4, respectively). In addition, SEs lacked the endoplasmic reticulum resident protein calreticulin. Lane 1 corresponds to a positive control (recombinant CD9 protein and HeLa cell and equine endothelial cell lysates for CD9, HSP70, and calreticulin, respectively).

and the RNA content was estimated in each individual sample. The average RNA content was 272.5 ng, with a range between 79.8 to 714 ng. Analysis of RNA size distribution using an Agilent Bioanalyzer along with an Agilent RNA 6000 Pico kit (Agilent Technologies, Santa Clara, CA) demonstrated that small RNAs were enriched in this sample type (Fig. 2A). Subsequently, we performed a nuclease protection assay to determine if SE-associated RNA is carried within intact exosomes. The nuclease protection assay demonstrated that 62% of the SE-associated RNA was protected from combined treatment with protease (pronase) and RNase digestion. Exosome lysis by detergent treatment, followed by protease and RNase digestions, resulted in an 80% reduction of total RNA content (Fig. 2B and C).

TABLE 1 Monoclonal and polyclonal antibodies specific to seminal exosomes and other exosomal markers used in this study[a]

Specificity	Species	Clone	Source
CD9	Mouse	MM2/57	AbD Serotec
CD63	Rabbit	NA	System Biosciences
CD81	Rabbit	NA	Santa Cruz Biotechnology
HSP70	Rabbit	NA	System Biosciences
Calreticulin	Rabbit	NA	Stressgen Biotechnologies Corp.
MHC-II	Mouse	CR3/43	Dako
Vimentin	Mouse	V9	Vector Laboratories

[a]NA, not applicable (polyclonal antibody); HSP70, heat shock protein 70; MHC-II, major histocompatibility complex class II.

In order to determine specific SE-associated RNA species and potential differences in their expression levels during EAV persistence, we performed miRNA sequencing on SEs derived from three stallions (L136, L139, and L140) at −30 (prechallenge) and 86 days postinfection (dpi) and from two EAV long-term persistently infected stallions (L136 and L140) at 726 dpi. The average numbers of total reads, mapped reads, mapped fractions, and reads per RNA biotype per sample type are shown in Tables 3 and 4. The large fraction of reads that did not map are largely attributed to rRNA fragments appearing as repeated sequences since the mapping algorithms (miRDeep2 [Max Delbrück Center, Berlin-Buch, Germany]) were set not to retain reads that mapped >5 times to the reference genome for analysis (frequently encountered with rRNA fragments). In the case of rRNAs and tRNAs, these represented a small fraction of the total mapped reads and constituted ≤3.2% of the total mapped reads in all samples analyzed. MicroRNAs were enriched in SE fractions, with an average number of reads of 2,360,732 ± 1,076,039 (mean ± standard deviation). A group of 23 miRNAs accounted for approximately 90% of the miRNA reads, of which 15 were shared in common between SE fractions collected at prechallenge, 86 dpi, and 726 dpi (Fig. 3; see also Table S1 in the supplemental material). The top five highly enriched miRNAs in SE fractions at those three time points included eca-let-7a-2, eca-let-7a, eca-mir-21, eca-let-7c, and eca-mir-10b. The mean percentages of the total miRNA reads are shown in Table 5. Together, these top five miRNAs accounted for a mean of 63.27% of the total miRNA reads.

Downregulation of SE-derived eca-mir-128 is associated with EAV long-term persistence in the stallion reproductive tract. MicroRNA sequencing data analysis identified a subset of 11 miRNAs that were differentially expressed in SEs during the course of EAV infection (Fig. 4A and Table 6). Six out of 11 miRNAs (eca-let-7e, eca-mir-34b, eca-mir-128-1, eca-mir-128-2 [the last two are referred to as eca-mir-128 since they present 100% identity in their mature sequence], eca-mir-132, and eca-mir-191a) showed an overall decrease in their expression levels during the course of EAV infection, while five (eca-mir-10a, eca-mir-28, eca-mir-146a, eca-mir-197, and eca-mir-885) conversely presented an increase in their expression levels (Fig. 4A and Table 6). Relative expression analysis by RT-qPCR of a larger number of samples comprising naive ($n = 15$), short-term carrier ($n = 7$), and long-term carrier ($n = 18$) stallions

TABLE 2 Expression of exosomal markers in SE fractions derived from naive ($n = 10$), EAV short-term carrier ($n = 5$), and long-term carrier ($n = 5$) stallions

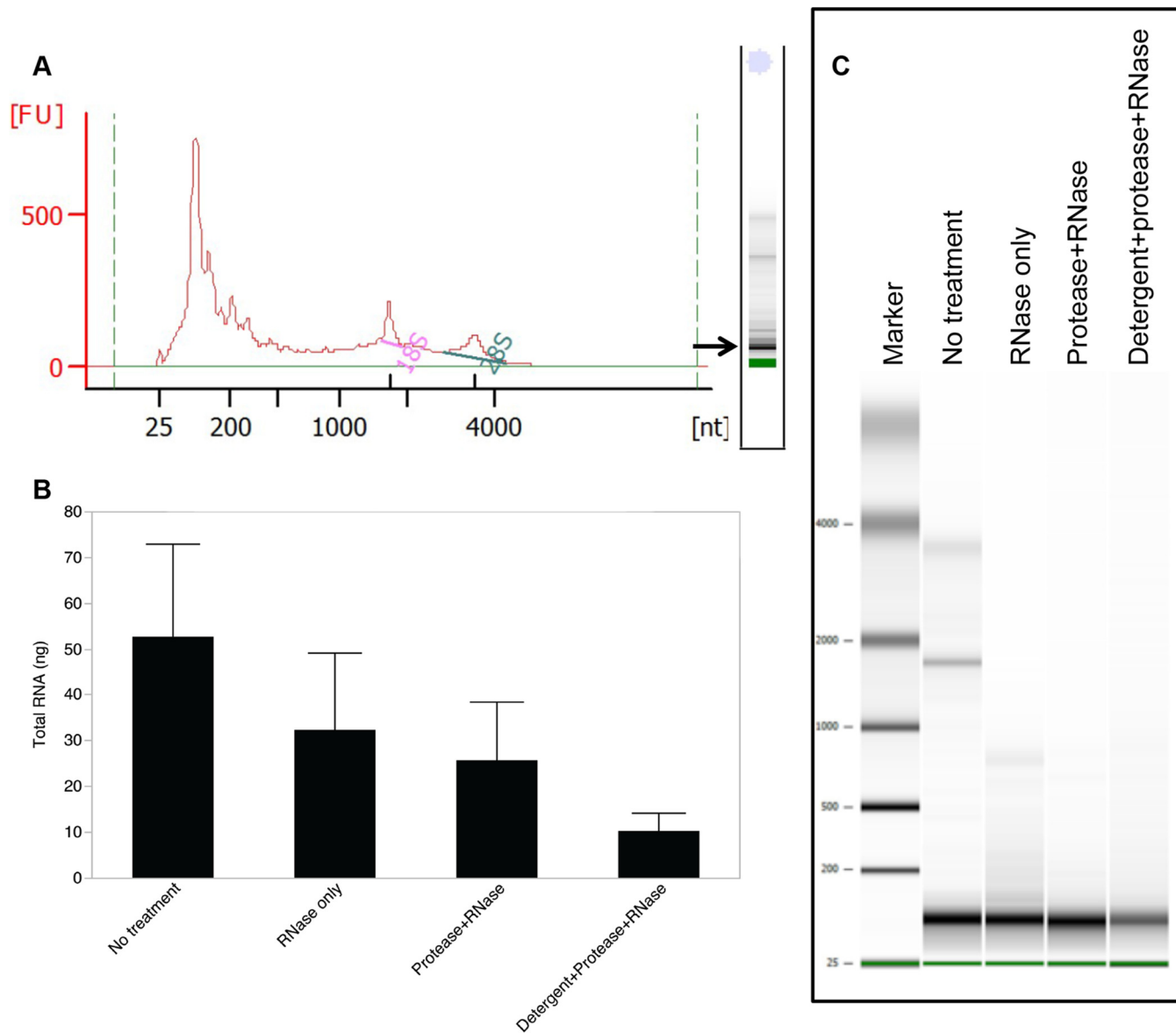| Exosomal marker	No. of positive SE samples/no. of SE samples tested		
	Naive	Short term	Long term
CD9	10/10	5/5	5/5
CD63	0/10	0/5	2/5
CD81	0/10	0/5	0/5
HSP70	10/10	5/5	5/5
Calreticulin	0/10	0/5	0/5
MHC-II	0/10	0/5	0/5
Vimentin	0/10	0/5	0/5

FIG 2 Equine SEs are enriched in small RNAs. (A) Bioanalyzer profile of seminal exosome fractions demonstrate enrichment of small RNAs (<200 bp; also see arrow on virtual electrophoresis in panel A). (B) A nuclease protection assay demonstrated that 62% of the RNA was protected from the combined treatment with protease, and RNase digestion and that exosome lysis by detergent treatment, followed by protease and RNase digestions, resulted in an 80% reduction of total RNA content. (C) Depiction of the virtual electrophoresis following sequential treatment of seminal exosomes during the nuclease protection assay.

confirmed a significant downregulation of eca-mir-128 (P value = 0.0011 and P value = 0.0106 for the pairwise comparisons between long-term carrier and naive or short-term carrier stallions, respectively) in the last group (Fig. 4B), while no statistically significant differences were observed between short-term carrier and naive stallions (P value = 0.9418). Subsequently, we analyzed the expression dynamics of eca-mir-128 in SEs sequentially collected during the course of EAV infection in two experimentally infected stallions (L136 and L140). While no significant differences were observed in the expres-

TABLE 3 Mean total reads, mapped reads, and mapped fractions in SEs

SE fraction	Mean total reads	Mean mapped reads	Mean mapped fraction (%)
Prechallenge	13,207,169 ± 1,780,999	5,993,444 ± 1,140,261	45.15 ± 3.05
86 dpi	13,431,616 ± 9,565,250	4,948,273 ± 3,345,532	38.46 ± 4.5
726 dpi	14,791,891 ± 3,331,733	5,924,778 ± 1,664,545	39.80 ± 2.29

TABLE 4 Mean total reads per RNA biotype identified in SE fractions

SE fraction	Mean miRNA reads	Mean tRNA reads	Mean rRNA reads	Mean mRNA reads
Prechallenge	2,744,802 ± 1,273,296	13,156 ± 8,639	26,181 ± 18,681	3,424,562 ± 1,405,618
86 dpi	2,133,247 ± 1,298,735	13,658 ± 9,556	10,050 ± 13,679	2,997,966 ± 2,043,063
726 dpi	2,125,853 ± 883,695	52,253 ± 12,358	127,762 ± 47,230	3,239,549 ± 1,077,548

sion of eca-mir-128 between prechallenge and 380 dpi, a significant downregulation of this miRNA was observed after 380 dpi (approximately 1 year postinfection; P values < 0.05). Furthermore, eca-mir-128 reached its lowest expression value by 726 dpi (Fig. 4C). No statistically significant differences were found for the other differentially expressed

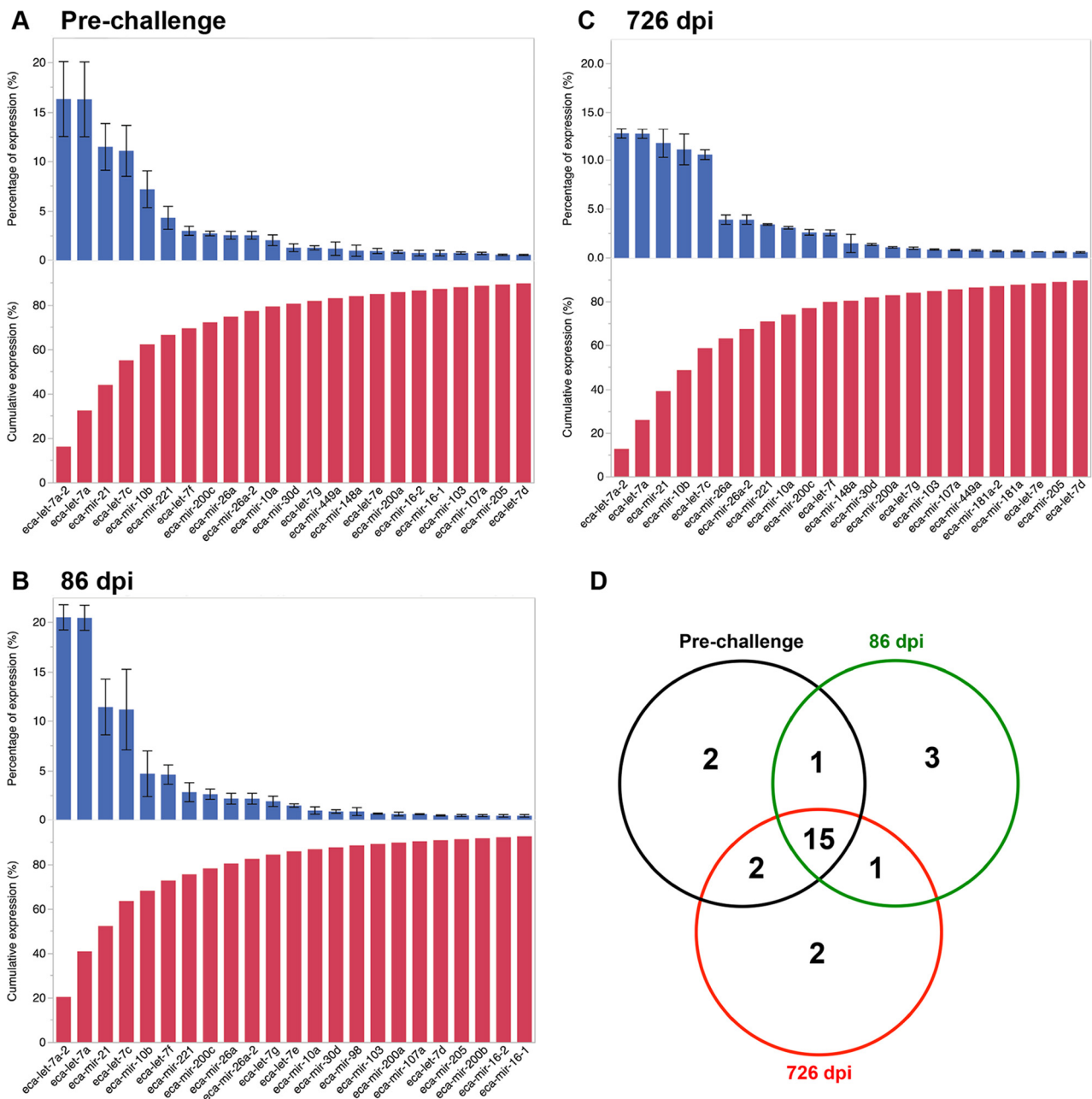**FIG 3** MicroRNAs that account for >90% of the total miRNA reads in SEs derived from naive (prechallenge) stallions and following equine arteritis virus infection. (A) Prechallenge; (B) 86 days postinfection; (C) 726 days postinfection. Mean percentages of expression ± standard errors of the means along with the cumulative expression are represented. (D) A total of 15/23 miRNAs were commonly shared across time points.

TABLE 5 Expression of the top 5 highly enriched miRNAs in SEs[a]

miRNA	Mean expression (%)
eca-let-7a-2	16.54 ± 3.88
eca-let-7a	16.51 ± 3.87
eca-mir-21	11.58 ± 0.17
eca-let-7c	10.96 ± 0.32
eca-mir-10b	7.67 ± 3.25

[a]The mean percentages of total miRNA reads ± standard deviation are shown.

miRNAs identified by miRNA sequencing between naive, short-term carrier, and long-term carrier stallions.

***CXCL16* constitutes a putative target of eca-mir-128.** Computational target prediction yielded a total of 805 putative target genes for eca-mir-128 (Table S2 in the supplemental material). Functional annotation analysis of target genes demonstrated their involvement in several biological processes, with a predominance of genes regulating metabolic and cellular processes but also involved in developmental, immune system, and reproduction processes, locomotion, adhesion, localization, and response to stimuli (Fig. 5A). Specifically, target genes were involved in regulation of gene expression, cell differentiation, development, and morphogenesis, protein phosphorylation and diverse signaling pathways, including the mitogen-activated protein kinase (MAPK) cascade, the phosphoinositide-3 kinase/protein kinase B (PI3K-Akt) signaling pathway, transforming growth factor (TGF) signaling, platelet-derived growth factor (PDGF) and epidermal growth factor (EGF) signaling, Hippo signaling, serine/threonine kinase signaling, ubiquitination, cell proliferation and apoptosis, DNA damage repair systems, and cell migration/chemotaxis (Table S3 in the supplemental material). Based on their molecular function and protein class, target genes were mainly involved in RNA/DNA/protein/metal binding, catalytic activity, transporter activity, receptor activity, structural activity, and signal transduction (Fig. 5B and C; see also Table S4 in the supplemental material). To analyze the functional relationships between eca-mir-128 target genes, we used PANTHER and DAVID bioinformatics tools. Pathway analysis performed by PANTHER retrieved 20 top pathways (P values < 0.05) potentially under the regulation of mir-128, and these are depicted in Table 7 and Fig. 6A. Among these, six were associated with immune pathways (Table 7). Pathway analysis demonstrated that mir-128 target genes may also be involved in inflammation mediated by chemokine/cytokine signaling, B and T cell activation, interleukin (IL) and TGF-β signaling, and apoptosis.

Interestingly, prediction tools identified *CXCL16* as a putative target of mir-128. Consequently, we predictively evaluated the miRNA-mRNA interaction between the mir-128 seed sequence and the 3' untranslated region (UTR) of its putative mRNA target, *CXCL16*. For this purpose, we analyzed the interaction between both the human and equine *CXCL16* 3' UTR and mir-128, respectively. Analysis of the human *CXCL16* 3' UTR by TargetScan predicted that the pairing region is located within nucleotides (nt) 664 and 670 of the 3' UTR (ACUGUGA) and that the hsa-mir-128-3p seed sequence is located between nt 1 and 7 (Fig. 6B). Prediction of the pairing region is consistent with a 7-mer-A1 site type, as it is a perfect match for the seed sequence of the mature miRNA and it is followed by an adenine. The miRNA-mRNA interaction between the human *CXCL16* 3' UTR sequence and mir-128 was determined to have a low free energy (ΔG = −19.2 kcal/mol). In the case of the equine *CXCL16* 3' UTR, miRNA-mRNA interaction analysis demonstrated that the mir-128 (nt 1 to 7) predicted pairing region comprises nt 37 to 43 of the 3' UTR (AUUGUGA) and that interaction occurs with a low free energy as well, estimated at −19.3 kcal/mol. Additionally, a guanine-uracil wobble occurs between nt 6 of mir-128 and nt 38 of the equine *CXCL16* 3' UTR (Fig. 6B).

***CXCL16* is upregulated in the ampullae of long-term EAV persistently infected stallions.** In order to establish an association between eca-mir-128 and its putative target, *CXCL16*, we evaluated the expression of the latter in the main site of EAV
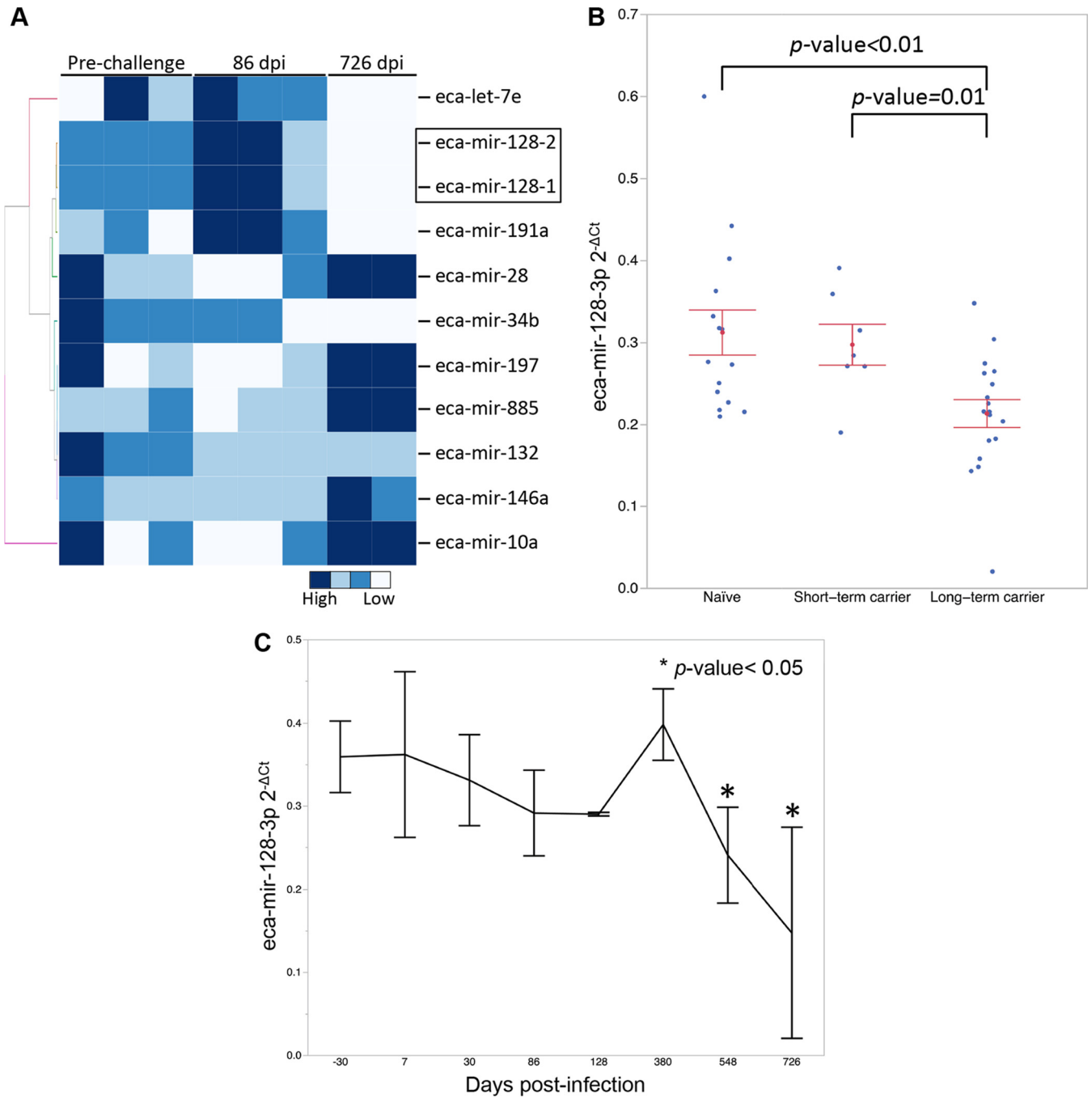
FIG 4 Differential expression analysis of miRNAs in seminal exosomes collected during the course of EAV infection (prechallenge and 86 and 726 days postinfection [dpi]). (A) Heat map depicting differentially expressed miRNAs identified in seminal exosomes by miRNA sequencing. The heat map was constructed using normalized read counts. A highly significant downregulation of eca-mir-128 can be observed in seminal exosomes derived from long-term persistently infected stallions ($n = 2$; 726 dpi; P value < 0.01) compared to values at prechallenge and 86 dpi. (B) Relative expression analysis of eca-mir-128 in seminal exosomes from naive ($n = 15$), short-term carrier ($n = 7$), and long-term carrier ($n = 18$) stallions revealed a significant downregulation of this miRNA in the last group (P value $= 0.0011$ and P value $= 0.0106$). Blue dots represent individual samples. (C) Kinetics of eca-mir-128 during EAV infection in long-term carrier stallions ($n = 2$). A significant downregulation of this miRNA was observed after 380 days postinfection.

persistence (i.e., ampullae) in the reproductive tract of the stallion (Fig. 7). *CXCL16*-specific TaqMan qPCR demonstrated a significant upregulation of *CXCL16* in the ampullae of both short-term ($n = 6$) and long-term persistently infected ($n = 3$) stallions compared to the naive group ($n = 4$; P values of 0.0279 and 0.0020, respectively; Fig. 7E). RNAscope *in situ* hybridization (ISH) and immunohistochemistry (IHC) were used to localize the expression of CXCL16 in the ampullae. CXCL16 expression was

TABLE 6 Differentially expressed miRNAs identified by miRNA sequencing analysis of SE fractions collected at prechallenge, 86 dpi, and 726 dpi[a]

miRNA	P value
eca-let-7e	0.033075 (86 dpi vs 726 dpi)
eca-mir-10a	0.03195 (86 dpi vs 726 dpi)
eca-mir-28	0.0312 (86 dpi vs 726 dpi)
eca-mir-34b	0.0208 (prechallenge vs 86 dpi)
	0.006 (prechallenge vs 726 dpi)
eca-mir-128-1	0.0045 (prechallenge vs 726 dpi)
	0.0033 (86 dpi vs 726 dpi)
eca-mir-128-2	0.0051 (prechallenge vs 726 dpi)
	0.00345 (86 dpi vs 726 dpi)
eca-mir-132	0.02865 (prechallenge vs 86 dpi)
eca-mir-146a	0.0267 (86 dpi vs 726 dpi)
eca-mir-191	0.01575 (86 dpi vs 726 dpi)
eca-mir-197	0.0402 (86 dpi vs 726 dpi)
eca-mir-885	0.02145 (86 dpi vs 726 dpi)

[a]P values are represented along with the time points that show significant differences, in parentheses. miRNAs that showed a significant downregulation associated with long-term EAV persistence are shown in bold. P values were subjected to a Benjamini-Hochberg correction and a false discovery rate (FDR) set at 0.05.

significantly abundant in the mucosal epithelial cells of the ampullae, primarily the luminal mucosal epithelium, as well as mucosal and submucosal lymphocyte and plasma cell infiltrates in long-term persistently infected stallions compared to short-term carrier and naive stallions (P values < 0.05 [Fig. 7A to C and 7E]), in which a lower expression of CXCL16 was observed in scattered epithelial cells (Fig. 7B and C). Furthermore, a significant negative correlation was observed between CXCL16 and SE eca-mir-128 expression levels ($\rho = -0.73$; P value = 0.0065 [Fig. 7E]).

DISCUSSION

The pathogenesis of persistent EAV infection in the male reproductive tract has been the subject of extensive investigation in recent years in our laboratory (26–28, 30, 31). We have demonstrated that long-term persistent infection in the stallion is associated with host genetic factors, specifically with the presence of a specific allele encoding the chemokine CXCL16 (CXCL16S) (30, 31). Furthermore, EAV has the ability to persist despite the induction of a strong systemic immune response and local inflammatory and mucosal antibody responses at the site of persistence (26, 27). Clearly, EAV employs complex strategies to evade host immunity, and the immunopathogenesis of viral persistence remains to be further elucidated (Fig. 8).

Since seminal plasma components have proven to have immunomodulatory effects that are necessary for fertility and may also influence the establishment of sexually transmitted diseases (34, 42, 48, 65–68), their role in enabling EAV persistence in the stallion warrants further investigation. In this study, we have specifically characterized the role of SE-associated miRNAs during EAV persistent infection since specific small RNA cargos within these extracellular vesicles can play a role in modulating local immunity, as recently suggested (34). Thus, we hypothesized that specific equine SE-associated miRNAs may modulate the local inflammatory response and, consequently, contribute to the establishment and maintenance of persistent EAV infection in the reproductive tract of the stallion. In this study, we sought to characterize the mature miRNA profile associated with SEs and to identify the specific miRNAs involved in the maintenance of EAV-persistent infection in the ampullae of persistently infected stallions.

Purified SEs were within the expected size range and were characterized by high expression of CD9, a ubiquitous exosome marker particularly enriched in prostasomes (34, 41, 64). In contrast to human SEs, we observed inconsistent expression of CD63 in equine SE fractions. Since SEs are derived from a number of tissues associated with the male reproductive tract, determining their specific origin constitutes a significant challenge. However, the lack of vimentin expression in SEs may suggest that these
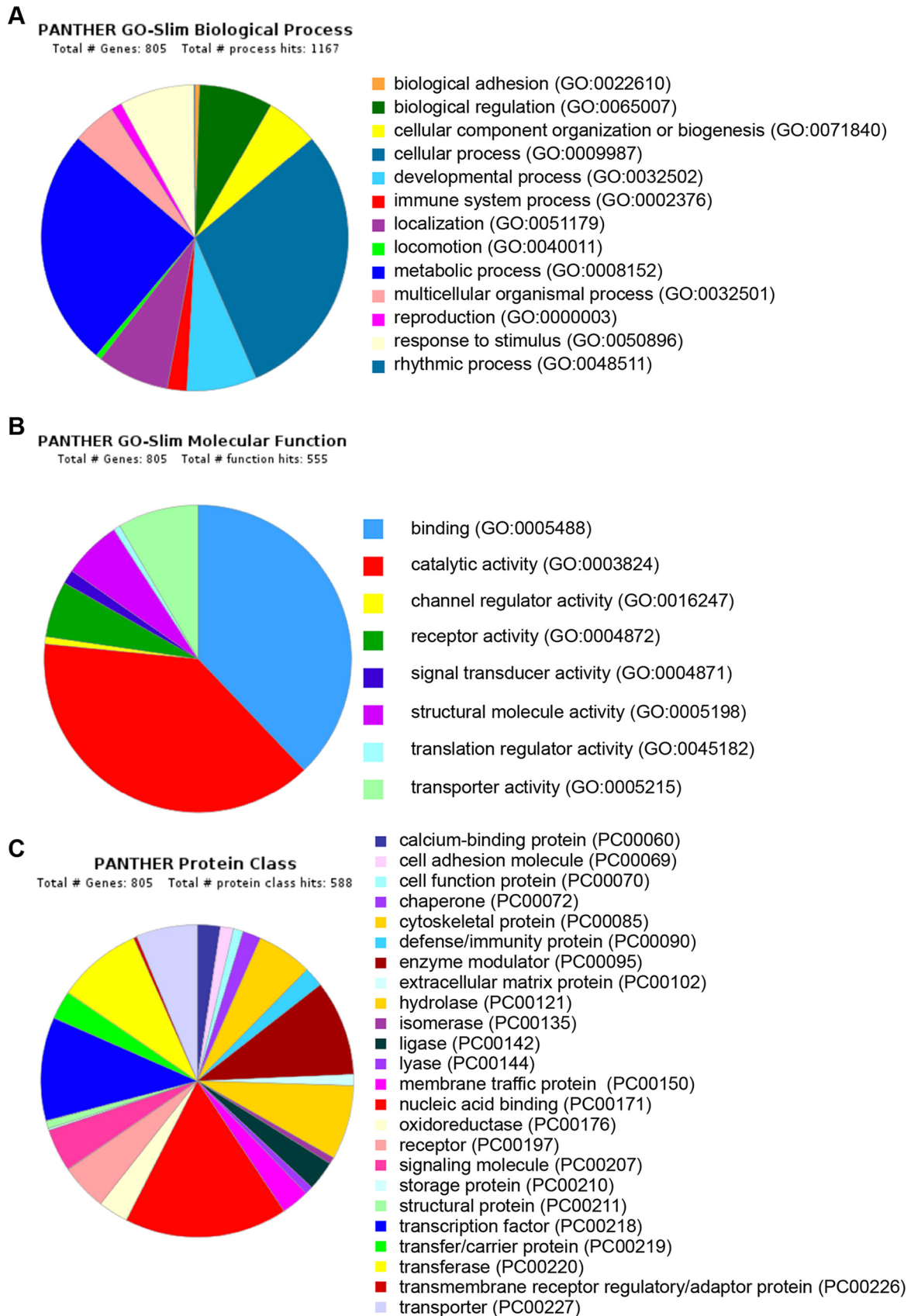
FIG 5 Functional annotation analysis of mir-128 target genes using PANTHER. A total of 805 putative target genes were classified according to their biological process (A), molecular function (B), and protein class (C).

TABLE 7 Top 20 significant pathways associated with eca-mir-128 target genes retrieved by PANTHER following the statistical overrepresentation test

PANTHER pathway	No. of targets	Fold enrichment	*P* value
PDGF signaling pathway (P00047)	15	2.63	8.26E−04
Gonadotropin-releasing hormone receptor pathway (P06664)	19	2.1	2.41E−03
CCKR signaling map (P06959)	15	2.26	3.40E−03
PI3 kinase pathway (P00048)	7	3.38	5.36E−03
Interferon gamma signaling pathway (P00035)	5	4.35	6.47E−03
Endothelin signaling pathway (P00019)	9	2.73	6.74E−03
Angiogenesis (P00005)	14	2.1	8.47E−03
Insulin/IGF pathway–mitogen-activated protein kinase kinase/MAP kinase cascade (P00032)	5	3.95	9.50E−03
Huntington disease (P00029)	12	2.2	9.94E−03
Ubiquitin proteasome pathway (P00060)	7	2.95	1.09E−02
Parkinson disease (P00049)	9	2.35	1.65E−02
Histamine H2 receptor-mediated signaling pathway (P04386)	4	4.01	1.87E−02
Insulin/IGF pathway-protein kinase B signaling cascade (P00033)	5	3.26	2.01E−02
Heterotrimeric G-protein signaling pathway–Gq alpha- and Go alpha-mediated pathway (P00027)	10	2.09	2.45E−02
p53 pathway (P00059)	8	2.29	2.60E−02
Histamine H1 receptor-mediated signaling pathway (P04385)	5	2.84	3.36E−02
Integrin signaling pathway (P00034)	13	1.75	3.96E−02
FAS signaling pathway (P00020)	4	3.07	4.33E−02
Enkephalin release (P05913)	4	2.98	4.72E−02
p53 pathway feedback loops 2 (P04398)	5	2.56	4.85E−02

extracellular vesicles are specifically shed by the lining epithelium of the reproductive tract rather than by cells of mesenchymal origin. Furthermore, Bioanalyzer profiling along with resistance to nuclease activity demonstrated that SEs are enriched in small RNAs and that their RNA repertoire mainly included mature miRNAs as well as other noncoding RNAs. It is noteworthy that when mature miRNA species predominant in equine SEs were analyzed by miRNA sequencing, we found that a small subset ($n = 23$) accounted for the vast majority of the miRNAs that were expressed, of which 15 were common to all the analyzed samples independently of infection status or interval after EAV infection. The top five miRNAs expressed in SEs included members of the let-7 family, mir-21 and mir10b, which have been demonstrated to play an active role in the modulation of several immune pathways, including modulation of T cell activation, NK cell function, IL-10 production by CD4$^+$ T lymphocytes, CD8$^+$ effector T lymphocyte differentiation, and NF-κB pathway, among others (69–74). From a confirmative viewpoint, these findings are similar to those reported for human SEs (34), suggesting that these miRNAs can be involved in similar modulatory processes in both species. Furthermore, the let-7 family of miRNAs as well as mir-21 are highly abundant in equine serum and plasma and also expressed in diverse tissue types (59, 75–80).

Validation of the miRNA sequencing data by RT-qPCR confirmed specific downregulation of eca-mir-128 in long-term persistently infected stallions, an intronic miRNA encoded by two distinct genes, eca-mir-128-1 and eca-mir-128-2, located on *Equus caballus* chromosome 16 (chr16:49087163– 49087246 [minus strand], corresponding to intron 16 or 18 of the cyclic AMP-regulated phosphoprotein 21-kDa gene [ARPP21], depending on the splice variant) and chromosome 18 (chr18:19492350– 19492419 [plus strand], corresponding to intron 22 of the R3H domain containing 1 gene [R3HDM1]), respectively. Similar to their human counterpart (hsa-mir-128), the mature sequences of both eca-mir-128-1 and eca-mir-128-2 are identical and conserved among species (81). While hsa-mir-128 has been extensively implicated in tumorigenesis (81), its role during viral infections and inflammatory processes has been less described (82–85). Recently, downregulation of eca-mir-128 has been implicated in
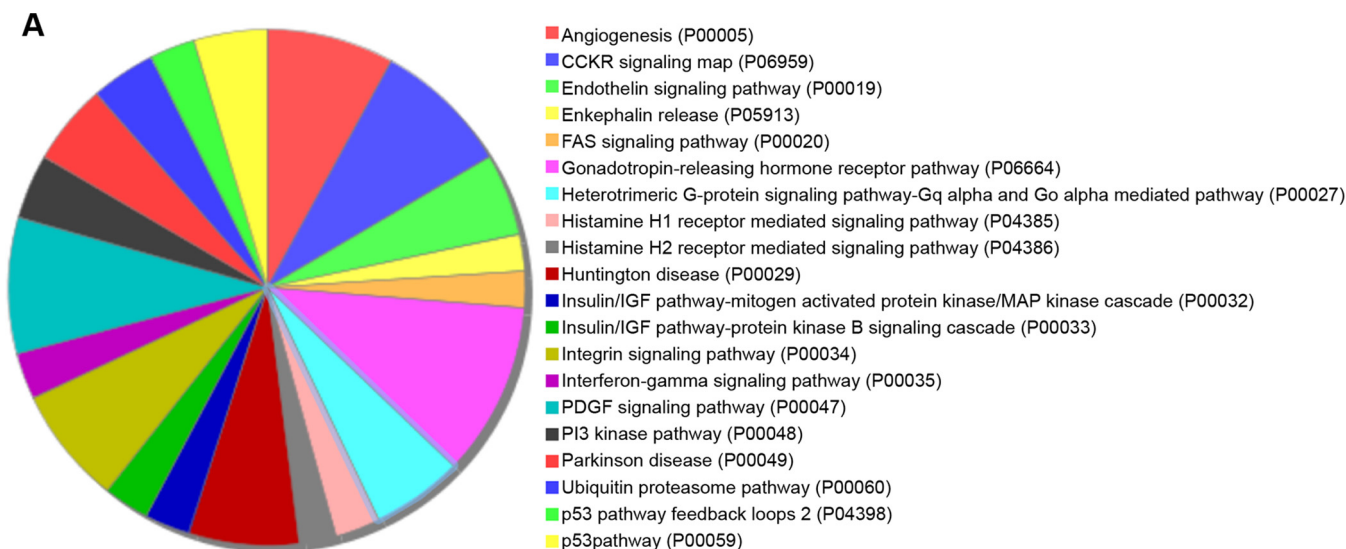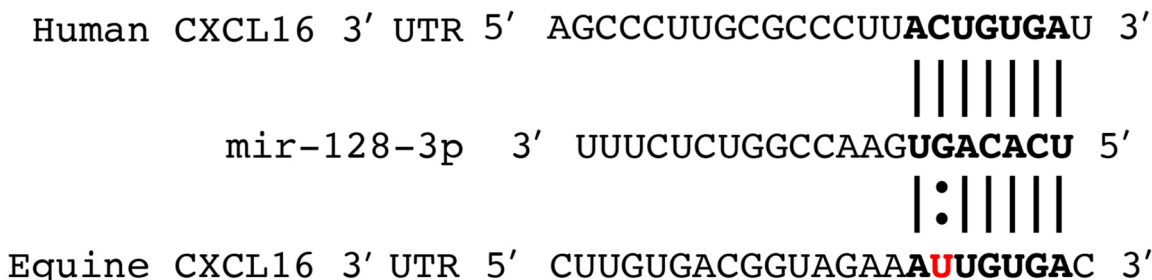
FIG 6 Pathway analysis of mir-128 target genes (*n* = 805) and comparative analysis of *CXCL16* 3′ UTR as a putative target of mir-128. (A) Pathway analysis by PANTHER retrieved a total of 20 significant pathways, which included pathways in common with the CXCL16/CXCR6 axis, such as PI3K-Akt, G-protein coupled receptor signaling, and some immune pathways. (B) Putative interaction between mir-128 and human and equine *CXCL16* 3′ UTR. The seed region of mir-128 and binding sites at the 3′ UTRs are in bold. The binding site is predicted as a 7-mer-A1 type, and in the horse sequence, a guanine-uracil wobble (marked in red) is predicted at nt 38 of the 3′ UTR. Both interactions occur with a low free energy (Δ*G* of −19.2 and −19.3 kcal/mol for the human and equine counterparts, respectively).

equine asthma and hypothetically related to the stimulation of allergic immune responses (82). In this study, we specifically determined that downregulation of SE eca-mir-128 is associated with long-term EAV persistence in the reproductive tract and that this specific miRNA is a putative regulator of *CXCL16* as determined by target prediction analysis. CXCL16, which belongs to the CXC chemokine family, acts as one of the cellular receptors of EAV and has been strongly implicated in EAV persistence in the reproductive tract (21, 30, 31, 86). The 3′ UTR and miRNA-mRNA interaction analysis predicted that the binding between the mir-128 seed sequence and its pairing region in the 3′ UTR of *CXCL16* mRNA occurs with low free energy, which indicates that the interaction is highly feasible. While the 3′ UTR binding site for human *CXCL16* is a perfect match with the mir-128 seed sequence, by comparison, the equine counterpart contains a guanine-uracil wobble. Nonetheless, wobble base pairing between the 3′ UTR binding site and the miRNA seed sequence has been previously reported and does not necessarily impact miRNA function (87–90). Moreover, eca-mir-128 expression kinetics during the course of infection in EAV long-term persistently infected stallions demonstrated that this miRNA is downregulated after approximately 1 year postinfection (380 dpi). To further understand the relationship between eca-mir-128 downregulation and its influence on CXCL16 expression in the reproductive tract, we evaluated the expression of CXCL16 in the primary EAV tissue reservoir (ampullae) of naive, short-term carrier, and long-term carrier stallions by RT-qPCR, RNAscope ISH, and IHC.
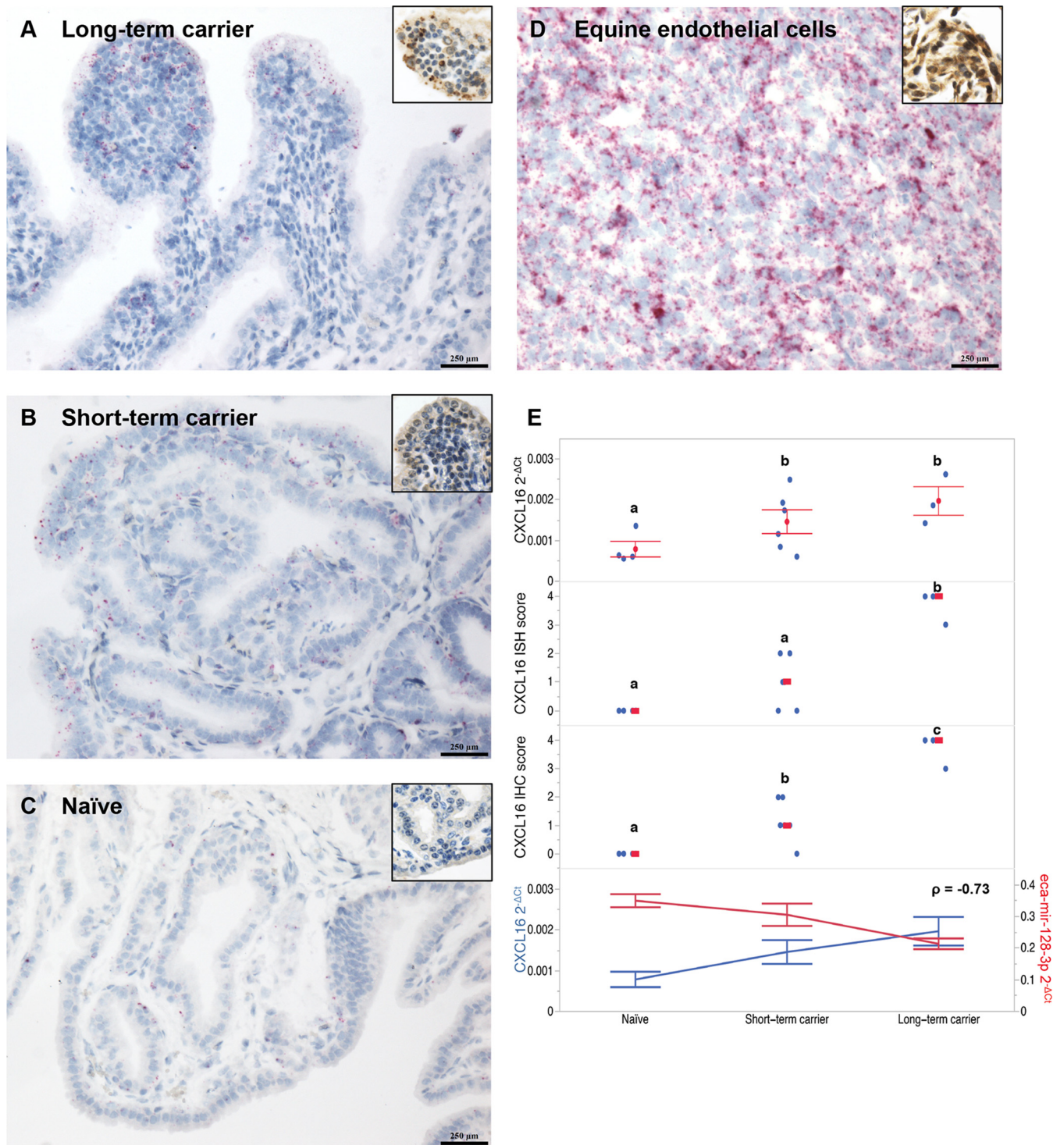
FIG 7 CXCL16 expression in the ampullae of EAV long-term carrier (n = 3), short-term carrier (n = 6), and naive (n = 4) stallions. (A to C) *CXCL16* is significantly upregulated in the ampullae of EAV long-term persistently infected stallions (A) compared to short-term carrier (B) and naive (C) stallions as determined by ISH and IHC (insets). *CXCL16* is predominantly expressed in the mucosal epithelium and lymphocytic infiltrates, especially in the luminal area. *CXCL16*-specific mRNA RNAscope ISH was performed with fast red; images are at a magnification of ×200. Bar = 250 μm. (Insets) An equine CXCL16-specific rabbit anti-peptide antibody was used for IHC. 3,3′-Diaminobenzidine tetrahydrochloride (DAB) stain was used; the image is at a magnification of ×400. (D) High expression of *CXCL16* in equine endothelial cell pellets as determined by *CXCL16*-specific RNAscope ISH and IHC (inset, DAB, ×400). Fast red was used; the image is at a magnification of ×200. Bar = 250 μm. (E) Higher expression of *CXCL16* in the ampullae of long-term carrier stallions (n = 3) was quantitatively determined by (top to bottom) TaqMan RT-qPCR, RNAscope ISH, and IHC, and it was demonstrated to be negatively correlated with SE eca-mir-128 expression. Blue dots represent values for individual stallions, while mean $2^{-\Delta CT}$ values ± standard errors of the means and median scores are represented in red. Letters indicate statistically significant differences between groups (P value < 0.05). For correlation analysis (E, bottom) between *CXCL16* and eca-mir-128 expression, mean $2^{-\Delta CT}$ values ± standard errors of the means are depicted.
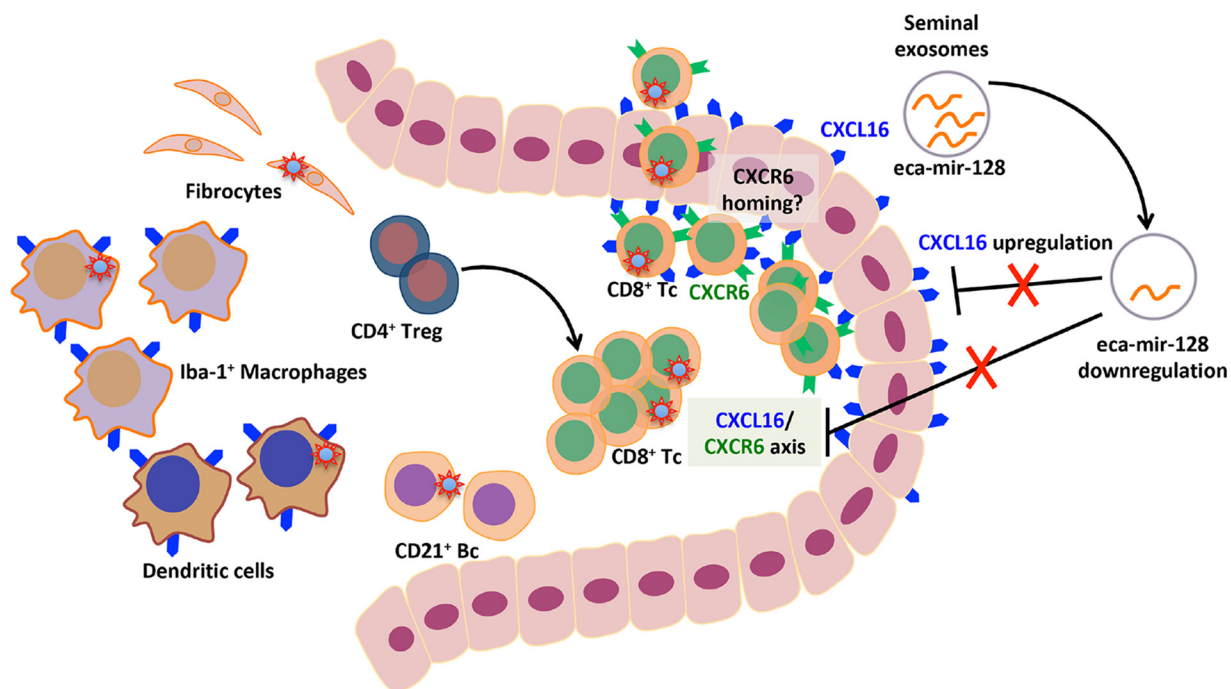
FIG 8 Schematic representation of the viral reservoir, inflammatory process, and role of the chemokine CXCL16 and eca-mir-128 during EAV long-term persistent infection in the reproductive tract of the stallion. EAV persistence is associated with CD8$^+$ T lymphocytes and CD21$^+$ B lymphocytes infiltrating the ampullae, fibrocytes, tissue macrophages, and dendritic cells. Long-term persistence is associated with a strong inflammatory response primarily mediated by CD8$^+$ T lymphocytes and a smaller population of CD4$^+$ T regulatory lymphocytes. Downregulation of SE eca-mir-128 is associated with enhanced expression of the chemokine CXCL16 in the mucosal epithelium and lymphocytes and thus modulates the CXCL16/CXCR6 chemokine axis. Expression of the CXCL16 receptor, CXCR6, is also upregulated in lymphocytes (Carossino and Balasuriya, unpublished), likely mediates specific homing of infected lymphocytes into the reproductive tract of the stallion and migration of these cells across the epithelial lining, and drives an immunologically unique microenvironment that favors viral persistence. CD8$^+$ Tc, CD8$^+$ T lymphocytes; CD4$^+$ Treg, CD4$^+$ T regulatory lymphocytes; CD21$^+$ Bc, CD21$^+$ B lymphocytes.

Differences in *CXCL16* expression levels between the three groups along with their negative correlation with eca-mir-128 expression levels demonstrated that long-term viral persistence induces the upregulation of this chemokine in the ampullae, providing further evidence of the key role that CXCL16 plays in the pathogenesis of EAV long-term persistent infection and indirectly suggesting that eca-mir-128 may regulate the expression of this gene in the reproductive tract and allow the establishment of viral persistence (Fig. 8). In this respect, it is possible that the delivery of specific miRNA cargos to epithelial and/or inflammatory cells in the reproductive tract mediated by SEs modulates specific target genes in specific cell populations as shown for other exosomes and, consequently, influences the local immune response (34, 91). It is likely therefore that eca-mir-128 dynamics in SEs influence the outcome of EAV infection in the reproductive tract. However, further *in vitro* experiments are required to confirm that equine *CXCL16* is a specific target for eca-mir-128. Additionally, eca-mir-128 is potentially involved in the regulation of several other pathways, some of which are associated with immune mechanisms (82, 83); thus, its role in local immune evasion mechanisms that allow EAV to persist deserves further investigation. The differential expression of the remaining set of miRNAs ($n = 9$) could not be confirmed, and the differences identified by miRNA sequencing could have been overestimated due to the very limited number of samples evaluated (two to three per time point) as well as the inclusion of diverse sequencing biases that can lead to enhancement or reduction of miRNA expression levels as previously reported (92).

Another significant finding from this study is that CXCL16 expression was not limited to inflammatory cells infiltrating the ampullae of long-term carrier stallions but was also abundant in the mucosal epithelium. Even though the mucosal epithelium expresses high levels of CXCL16, recent studies demonstrated that virus is not harbored in the

epithelial cells of the ampullae or other accessory sex glands (26). This observation is supportive of the fact that ongoing studies in our laboratory suggest that EAV requires additional cellular entry factors, among which vimentin seems to play an important role (S. Sarkar and U. B. R. Balasuriya, unpublished data). Thus, the lack of vimentin expression in the mucosal epithelium may be a determinant for the lack of susceptibility of CXCL16$^+$ epithelial cells in the ampullae to EAV infection (26).

In conclusion, the study presented here provides insight into the miRNA species associated with SEs in the stallion and, most importantly, identified the specific downregulation of SE eca-mir-128 during long-term EAV persistent infection in the reproductive tract, a miRNA that predictively targets *CXCL16*. This study has also unequivocally demonstrated that upregulation of CXCL16 in the reproductive tract is associated with the establishment of long-term viral persistence, providing a strong link between the genetic studies undertaken and the pathogenesis of persistent EAV infection. While the evidence provided by this study indirectly suggests that SE eca-mir-128 modulates the expression of CXCL16 in the reproductive tract, further studies to confirm these observations are warranted (Fig. 8). In addition, other ongoing studies in our laboratory strongly suggest that EAV exploits the CXCL16/CXCR6 chemokine axis in order to modulate local inflammatory and immune responses at the site of persistent infection and that this chemokine axis is probably involved in specific homing of infected lymphocytes into the reproductive tract (M. Carossino and U. B. R. Balasuriya, unpublished data). Interestingly, it is yet to be uncovered how other eca-mir-128 regulated pathways contribute to modulating the CXCL16/CXCR6 axis favoring long-term EAV persistent infection in the stallion reproductive tract. In summary, this study advances our current understanding of EAV persistent infection and demonstrates that diverse and complex host factors are involved in the modulation of viral persistence in the stallion reproductive tract.

MATERIALS AND METHODS

Semen samples. Collection of equine semen samples from stallions that were experimentally infected with EAV ($n = 7$) has been described elsewhere (19, 26, 27). In addition, archived semen samples from long-term EAV carrier stallions that were naturally infected with EAV were included in the study. These semen samples had been submitted to the OIE Reference Laboratory at the Maxwell H. Gluck Equine Research Center for monitoring EAV carrier state following natural EAV infection in the field. A total of 53 semen samples derived from naive stallions ($n = 16$), short-term carrier stallions ($n = 7$), and long-term carrier stallions ($n = 30$, which include sequential semen samples from two long-term persistently infected stallions [726 dpi] to evaluate eca-mir-128 dynamics) were included in the study. For short-term carrier stallions (duration of viral shedding $<$ 1 year), semen samples collected 1 year following viral clearance were used. In the case of long-term carrier stallions (duration of viral shedding $\geq$ 1 year), semen samples collected 2 years postinfection were used. All the semen samples were stored in 1-ml aliquots at -80 °C.

Animal care and ethics. This study was performed in strict accordance with the recommendations in the *Guide for the Care and Use of Laboratory Animals* of the National Research Council (93). The Institutional Animal Care and Use Committee (IACUC) at the University of Kentucky, Lexington, KY, approved this protocol (number 2011-0888). Stallions were humanely euthanized by pentobarbital overdose following the American Veterinary Medical Association (AVMA) guidelines for the euthanasia of animals, and all efforts were made to minimize suffering.

Tissue samples. Tissue samples (ampullae) derived from a group of naive stallions ($n = 4$), EAV experimentally infected stallions ($n = 8$), and an EAV naturally infected stallion ($n = 1$) were used in this study (26). These were aseptically collected during postmortem examination and archived at -80 °C or formalin fixed and paraffin embedded (FFPE) as previously described (26).

Isolation of seminal exosomes. Before SE isolation, semen samples were thawed on ice and centrifuged at 3,000 $\times$ *g* for 15 min at 4°C to remove cellular debris. The seminal plasma was subsequently filtered through a 0.8-μm filter (EMD Millipore, Billerica, MA). Seminal exosome isolation was carried out using ExoQuick exosome precipitation solution (System Biosciences, Palo Alto, CA). Briefly, 126 μl (63 μl per 250 μl of biofluid as recommended by the manufacturer) of the ExoQuick exosome precipitation solution was added to 500 μl of filtered seminal plasma, mixed, and incubated overnight (minimum of 12 h) at 4°C to allow SE precipitation. Finally, the mixture was centrifuged at 1,500 $\times$ *g* for 30 min at 4°C, the supernatant was removed, and the exosome pellet was either used for downstream applications or stored at -80°C.

Antibodies. A panel of monoclonal and polyclonal antibodies specific for various exosome markers was used for characterization of SEs by TEM/immunogold labeling and Western immunoblotting analysis (Table 1). An equine CXCL16-specific rabbit anti-peptide antibody (86) was used for immunohistochemical (IHC) staining. Secondary antibodies conjugated to horseradish peroxidase (HRP; goat anti-mouse

IgG [H+L]-HRP and goat anti-rabbit IgG [H+L]-HRP [SouthernBiotech, Birmingham, AL]) were used for Western immunoblotting. A secondary antibody conjugated to 12-nm colloidal gold (goat anti-mouse IgG [H+L] [Jackson ImmunoResearch Laboratories, Inc., West Grove, PA]) was used for immunogold labeling. The Bond Polymer Refine Detection kit (Leica Biosystems, Buffalo Grove, IL) was used for IHC.

Transmission electron microscopy and size determination of seminal exosomes. SEs isolated from prechallenged semen samples collected from two naive stallions were used for TEM and immunogold labeling (see below). Briefly, purified SE pellets obtained using the ExoQuick exosome precipitation solution were resuspended in 1/10 of the original volume (50 μl) of phosphate-buffered saline (PBS; pH 7.4; Gibco, Carlsbad, CA) and fixed at a 1:1 ratio in 4% paraformaldehyde for 30 min at room temperature. Subsequently, a Formvar-carbon coated 400-mesh copper grid was floated on a 40-μl drop of the SE fractions for 15 min at room temperature to allow SE adsorption. Excess sample was drained off, and the grids were washed on a drop of Tris-buffered saline (TBS; pH 7.4) for 10 min at room temperature, followed by rinsing once in deionized water. Grids were finally contrasted on a drop of 3% aqueous phosphotungstic acid (pH 7.0) for 2 min, excess stain was removed using filter paper, and grids were observed under a JEOL JEM-1011 transmission electron microscope (University of Georgia Electron Microscopy Services, College of Veterinary Medicine, Athens, GA). Digital images were acquired with an XR80M wide-angle multidiscipline mid-mount charge-coupled-device (CCD) camera (Advanced Microscopy Techniques Corp., Woburn, MA). SE size distribution was assessed by taking measurements using the TEM imaging software.

Immunogold labeling. Purified SE pellets obtained using the ExoQuick exosome precipitation solution were resuspended and fixed as described above. Subsequently, a Formvar-carbon coated 400-mesh nickel grid was floated on a 40-μl drop of the SE fractions for 15 min at room temperature to allow SE adsorption. Excess sample was drained off, and the grids were washed on a drop of TBS (pH 7.4) for 10 min at room temperature and subsequently blocked in TBS containing 2% bovine serum albumin (BSA) for 30 min at room temperature. The grids were incubated with mouse anti-CD9 (1:50 dilution; Table 1) for 1 h at room temperature using a spotting dish in a wet chamber. Excess primary antibody was extensively washed using blocking buffer, followed by secondary antibody incubation (goat anti-mouse IgG conjugated with 12-nm colloidal gold; 1:20 dilution) for 30 min at room temperature using a spotting dish in a wet chamber. Grids were extensively washed in blocking buffer and finally rinsed in deionized water. Grids were contrasted with 3% aqueous phosphotungstic acid (pH 7.0) and visualized as indicated above.

Western immunoblotting. Seminal plasma samples from naive ($n = 10$), short-term carrier ($n = 5$), and long-term carrier ($n = 5$) stallions were evaluated by Western immunoblotting. Purified SE pellets obtained using the ExoQuick exosome precipitation solution were resuspended in 100 μl of 1× radioimmunoprecipitation assay (RIPA) buffer (Santa Cruz Biotechnology, Dallas, TX) containing Halt protease inhibitor cocktail (Thermo Fisher Scientific, Waltham, MA), vortexed for 15 s, and incubated for 5 min at room temperature for complete lysis. The protein concentration of the lysates was determined using a spectrophotometer (optical density [OD] at 280 nm; NanoDrop 2000 spectrophotometer; Thermo Fisher Scientific). A total of 30 μg of total protein was resuspended in 2× Laemmli sample buffer (Bio-Rad, Hercules, CA) containing 2-mercaptoethanol (Sigma-Aldrich, St. Louis, MO; except for CD9 detection), boiled at 95°C for 5 min, and subjected to denaturing polyacrylamide gel electrophoresis (SDS-PAGE) on a 12% resolving and 4% stacking gel. Subsequently, SE proteins were wet transferred onto a polyvinylidene difluoride (PVDF) membrane (Bio-Rad) for 1 h at 4°C. Transferred PVDF membranes were briefly washed in TBS (pH 7.6) containing 0.05% Tween 20 (TBS-T; Bio-Rad) and blocked with 5% skim milk in TBS-T for 1 h at room temperature. Membranes were incubated with the primary antibody (diluted at a concentration of 1 μg/ml in blocking buffer) overnight at 4°C with gentle rocking and washed 3 times for 10 min each time with TBS-T. The membranes were incubated with the respective secondary anitbody (goat anti-mouse or goat anti-rabbit conjugated to HRP diluted 1:5,000 in blocking buffer) for 1 h at room temperature with gentle rocking. After subsequent washes, membranes were developed using SuperSignal West Pico chemiluminescent substrate (Thermo Fisher Scientific) as indicated by the manufacturer. Developed membranes were imaged using an Azure c300 digital imager system (Azure Biosystems, Dublin, CA). Specific positive controls were run in parallel for each primary antibody.

RNA isolation. Exosomal RNA was isolated from purified SE pellets using the SeraMir exosome RNA isolation kit (System Biosciences) according to the manufacturer's instructions. RNA yield was determined by fluorometry (Qubit RNA HS assay kit; Thermo Fisher Scientific), and size distribution was assessed using an Agilent RNA 6000 Pico kit (Agilent Technologies, Inc.) according to the manufacturer's instructions. Additionally, total RNA was isolated from the ampullae for RT-qPCR. Briefly, 50 mg of tissue was dissected, placed in 1 ml of QIAzol lysis reagent (Qiagen, Valencia, CA), and homogenized using MagNA Lyser green beads (Roche, Indianapolis, IN) in a Bead Ruptor 12 (Omni International, Inc., Kennesaw, GA). Lysates were incubated for 5 min at room temperature, followed by addition of 200 μl of chloroform (Sigma-Aldrich). The upper aqueous phase was transferred into a new tube following centrifugation (12,000 × g for 15 min at 4 °C), and 1 volume of 70% ethanol was added. RNA isolation was finally performed using the RNeasy minikit (Qiagen) according to the manufacturer's recommendations.

Nuclease (RNase) protection assay. Purified SE pellets derived from 1 ml of seminal plasma were resuspended in 200 μl of nuclease-free 1× PBS (pH 7.4; Ambion, Thermo Fisher Scientific) and divided into four equal fractions, each receiving one of the following treatments: (i) no treatment, (ii) RNase treatment only, (iii) protease followed by RNase treatment, and (iv) detergent followed by protease and RNase treatment. Detergent treatment was performed with 1% NP-40 (Thermo Fisher Scientific) for 15

min on ice. Fractions subjected to protease treatment were incubated with pronase (600 μg/ml; Roche) for 20 min at 40°C, followed by enzyme inactivation at 80°C for 15 min. Finally, fractions subjected to RNase treatment were incubated for 30 min at 37°C with Ambion RNase cocktail enzyme mix (final concentrations of 12 U/ml of RNase A and 500 U/ml of RNase T1; Thermo Fisher Scientific). Following treatment, exosomal RNA was isolated as indicated above, and its yield and size distribution were assessed using an Agilent RNA 6000 Pico kit (Agilent Technologies, Inc.). The percentage of protected RNA was estimated after three treatment replicates.

MicroRNA library preparation and NGS. To determine the miRNA profile in SEs from naive as well as EAV persistently infected stallions, RNA was isolated from 8 SE samples (L136, prechallenge, 86 dpi, and 726 dpi; L140, prechallenge, 86 dpi, and 726 dpi; and L139, prechallenge and 86 dpi). The exosomal RNA was isolated as described above and submitted to System Biosciences for next-generation sequencing (NGS) (miRNA sequencing). Briefly, the NGS libraries were generated with TailorMix MicroRNA Sample Preparation version 2 (SeqMatic LLC, Fremont, CA). The 3′ adaptors were ligated to each RNA sample, and excess 3′ adaptors were subsequently removed. Subsequently, the 5′ adaptors were then ligated to the 3′ adaptor-ligated samples, followed by first-strand cDNA synthesis from the ligated products. The cDNA library was amplified and barcoded via enrichment PCR. The final RNA library was size selected on an 8% Tris-borate-EDTA (TBE) polyacrylamide gel. Sequencing was performed on the Illumina NextSeq 500 platform (1 × 75-bp single-end reads).

MicroRNA sequencing data analysis. The raw FASTQ files for each sample were trimmed three times with Trim Galore (Babraham Institute, Cambridge, UK). The trimmed FASTQ files were converted to FASTA format as required for using miRDeep2 (94). miRDeep2 produced an ARF file with the mapping details of all the reads that could be mapped to the *Equus caballus* reference genome (EquCab2.0) (95). If a read was mapped to >5 different locations in the reference sequence (-r setting in miRDeep2), it was not included in the mapped data set for analysis. Known miRNAs for *Equus caballus* were downloaded from miRBase (release 21) (96, 97). Many of the mapped reads could be assigned to either known equine miRNAs or tRNAs as described in the Genomic tRNA database (GtRNAdb) (98). The remaining mapped sequences were compared to the Ensembl annotation for the horse in order to identify mRNA and rRNA fragments. MicroRNA read counts were normalized using the formula log {[(reads × 1,000,000)/total reads] + 1} (79). For further analysis, miRNAs with at least three read counts in every sample were used.

Prediction of miRNA target genes. miRDB, TarBase v7.0 and the miRSearch target prediction tool (Exiqon, Woburn, MA) were used for miRNA target predictions (99, 100). Those genes with a target score of ≥80 (miRDB) or ≥0.4 (TarBase) were selected for further analysis. In addition, miRTarBase was used for identification of validated target genes (101). Analysis and identification of mir-128 binding site at the 3′ UTR of human and equine *CXCL16* mRNA (GenBank accession numbers NM_022059.3 and XM_001504756.5, respectively) was performed using TargetScanHuman release 7.1 (102) and IntaRNA 2.0 (Freiburg RNA Tools, Universität Freiburg, Germany) (103). The free energy (ΔG) of the predicted miRNA-mRNA interaction was estimated using the RNAhybrid tool (Universität Bielefeld, Germany) (104). A ΔG cutoff value of ≤−15 kcal/mol was used to assess the feasibility of the miRNA-mRNA interaction as previously suggested (105).

Functional annotation and pathway analysis. To investigate the molecular and biological functions of predicted miRNA target genes, DAVID Bioinformatics Resources (version 6.8 [https://david.ncifcrf .gov/], National Institute of Allergy and Infectious Disease [NIAID], National Institutes of Health [NIH] [106, 107]) along with the PANTHER classification system (http://www.pantherdb.org) (108) was used to functionally annotate genes based on gene ontology (biological process, molecular function, and protein class) and perform pathway analysis.

MicroRNA quantitative real-time PCR. Expression levels of differentially expressed miRNAs identified by miRNA sequencing between any of the sequenced time points (prechallenge, 86 dpi, and 726 dpi) were determined by RT-qPCR. For this purpose, seminal plasma samples from naive ($n = 15$), short-term carrier ($n = 7$), and long-term carrier ($n = 18$) stallions were used. Among the samples derived from long-term carrier stallions ($n = 18$), two were derived from experimentally infected stallions described elsewhere (L136 and L140), while the remaining samples corresponded to naturally infected stallions which have been monitored for >5 years following infection by the OIE Reference Laboratory (Maxwell H. Gluck Equine Research Center). Additionally, sequential semen samples from the two experimentally infected stallions ($n = 12$) were used to evaluate eca-mir-128 expression dynamics. Exosomal RNA was reverse transcribed using the miScript II RT kit (Qiagen) following the manufacturer's recommendations. For reverse transcription of mature miRNA, 10 ng of exosomal RNA was combined with 5× miScript HiSpec buffer (4 μl), 10× miScript Nucleics mix (2 μl), and miScript reverse transcriptase mix (2 μl). The final reaction volume was 20 μl. The reaction mixture was incubated at 37°C for 1 h, followed by inactivation of the reverse transcriptase at 95°C for 5 min. cDNA was diluted 1:5 in nuclease-free water, aliquoted, and stored at −20°C until used. For qPCR, the miScript SYBR green PCR kit (Qiagen) was used. Briefly, 1 μl of cDNA was added to a reaction volume (9 μl) containing 2× QuantiTect SYBR green PCR master mix (5 μl), 10× miScript universal primer (1 μl), assay-specific primers (1 μl of a 5 μM stock; final concentration, 0.5 μM), and RNase-free water (2 μl). The cycling conditions included an initial PCR activation step (95°C for 15 min) followed by 40 cycles of denaturation at 94°C for 15 s, annealing at 55°C for 30 s, and extension at 70°C for 30 s. Melt curve analysis was performed to check for nonspecific amplifications along with the inclusion of nontemplate controls. MicroRNA-specific forward primers were designed using miRprimer v2.0 (see Table S5 in the supplemental material) (109, 110). qPCR efficiencies and threshold cycle (C_T) values were determined using LinRegPCR v2017.0 (111), with efficiencies in the range of 90.2 to 100.2%. C_T values of >37 were not used for analysis. MicroRNA expression levels were normalized to three housekeeping miRNAs (eca-mir-30d, eca-mir-93, and eca-

mir-103/eca-mir-107a), which were selected using NormFinder v20 to identify those miRNAs with the most consistent expression pattern across samples (79, 112). MicroRNA expression levels were finally expressed as $2^{-\Delta CT}$.

CXCL16 quantitative real-time PCR. CXCL16 expression in the ampullae was evaluated by TaqMan quantitative real-time PCR. Reverse transcription was performed using a high-capacity cDNA reverse transcription kit (Thermo Fisher Scientific) following the manufacturer's recommendations. The reaction (20 μl) included 10 μl of total RNA (2 μg), 2 μl of 10× RT buffer, 0.8 μl 25× deoxynucleotide triphosphate (dNTP) mix (100 mM), 2 μl of 10× RT random primers, 1 μl of MultiScribe reverse transcriptase, 1 μl of RNase inhibitor, and 3.2 μl of nuclease-free water. The reverse transcription reaction mixture was incubated for 10 min at 25°C, followed by 120 min of incubation at 37°C and a final step at 85°C for 5 min. cDNA was diluted 1:1 in nuclease-free water and stored at −20°C until used. A custom TaqMan gene expression assay was developed for equine CXCL16 by a commercial company (Thermo Fisher Scientific) using the mRNA sequences derived from GenBank accession number XM_001504756.5. Each 10-μl qPCR mixture consisted of 4.5 μl of cDNA and 5.5 μl of master mix, which included 5 μl of TaqMan gene expression master mix (Thermo Fisher Scientific) and 0.5 μl of the custom TaqMan gene expression primer-probe mix (5′ fluorescein amidite [6-FAM] labeled). The cycling conditions included a holding step at 50°C for 2 min and an activation step at 95°C for 10 min, followed by 40 cycles of denaturation (95°C for 15 s) and annealing/extension (60°C for 1 min). RT-qPCR efficiencies and C_T values were determined as indicated above, and expression levels were normalized to those of three housekeeping genes (GAPDH, ACTB, and GUSB) and analyzed as indicated above.

CXCL16-specific ISH (RNAscope) and immunohistochemistry (IHC) assays. A CXCL16 mRNA-specific probe based on GenBank accession number XM_001504756.5 was developed by a commercial company (Advanced Cell Diagnostics [ACD], Newark, CA) and contained a total of 16 double Z-branched DNA probe pairs spanning a target region of 730 bp of the mRNA sequence (nt 598 to 1328). The probe was supplied in a ready-to-use format, and its specificity was evaluated using lymphoid tissues (palatine tonsils) and an equine endothelial cell line known to abundantly express CXCL16 (Fig. 7D). Probes specific to dihydrodipicolinate reductase B mRNA of *Bacillus subtilis* and peptidylprolyl isomerase B (PPIB) were used as negative and positive controls to assess assay specificity and RNA integrity in FFPE tissues, respectively. The RNAscope *in situ* hybridization (ISH) assay was performed using the RNAscope 2.0 HD red detection kit (ACD, Hayward, CA) as previously described, with some modifications (113), which included a second pretreatment for 15 min (100 to 104°C) and a third pretreatment for 20 min (40°C). The signal was finally detected using a fast red solution (red B and red A in a 1:60 ratio) for 10 min at room temperature. Slides were counterstained with 50% Gill hematoxylin I (American MasterTech Scientific, Lodi, CA) for 2 min, bluing was performed with 0.02% ammonium hydroxide in water, and sections were finally dried and mounted using EcoMount (Biocare Medical, Pacheco, CA). The ISH signal in the region of interest was quantified per the manufacturer's recommendations as follows: 0, no staining or <1 dot every 10 cells at a magnification of ×40; 1, 1 to 3 dots every 10 cells at a magnification of ×40; 2, 4 to 10 dots/cell (visible at a magnification of ×20 to ×40); 3, >10 dots/cell, with scattered cells presenting dot clusters (visible at a magnification of ×20); and 4, >10 dots/cell, with frequent cells presenting dot clusters (visible at a magnification of ×20).

For IHC, sections of FFPE tissues (5 μm) were mounted on positively charged Superfrost Plus slides (Fisher Scientific, Pittsburgh, PA) and processed as previously described (26). Heat-induced epitope retrieval was performed using a modified citrate-based ready-to-use solution (pH 6.1; Dako, Carpinteria, CA) as described previously (26), and immunostaining was performed using the Bond Polymer Refine Detection kit (Leica Biosystems, Buffalo Grove, IL). The slides were incubated with 3% hydrogen peroxide (5 min), followed by incubation with CXCL16-specific rabbit antipeptide sera (diluted 1:1,000 in ISH/IHC Super Blocking [Leica Biosystems]) for 1 h at room temperature. This was followed by incubation with a polymer-labeled goat anti-rabbit IgG conjugated to HRP (8 min). 3,3′-Diaminobenzidine tetrahydrochloride (DAB) was used as the substrate, and the slides were incubated for 10 min. Finally, sections were counterstained with hematoxylin and mounted as previously described (26, 27, 113). Immunostaining was qualitatively scored based on the staining intensity within the region of interest (0, no staining; 1, minimal staining; 2, mild staining; 3, moderate staining; 4, high staining).

Statistical analysis. Data distribution, descriptive statistics, plots, and statistical tests were generated using JMP11 Pro statistical analysis software and SAS (SAS, Cary, NC). Heat maps were built using package d3heatmap in R. A one-way analysis of variance (ANOVA) was used to identify differentially expressed miRNAs (SAS), followed by a Benjamini-Hochberg correction. RT-qPCR data ($2^{-\Delta CT}$ values) were analyzed using ANOVA (JMP11 Pro), and *post hoc* comparisons were performed using the Student *t* test (114). ISH and IHC scores were subjected to a nonparametric test (Kruskal-Wallis) using JMP11 Pro. Correlation analysis between CXCL16 $2^{-\Delta CT}$ and eca-mir-128 $2^{-\Delta CT}$ values was performed by the Spearman rank correlation method. Statistical significance was set at a P value of <0.05 in all cases.

Accession number(s). The RNA sequencing data from this study were deposited in the Gene Expression Omnibus (GEO, NCBI, NIH) database under study GSE108180 (accession numbers GSM2891902 to GSM2891909).

SUPPLEMENTAL MATERIAL

Supplemental material for this article may be found at https://doi.org/10.1128/JVI .00015-18.

SUPPLEMENTAL FILE 1, XLSX file, 0.1 MB.
SUPPLEMENTAL FILE 2, XLSX file, 0.1 MB.

SUPPLEMENTAL FILE 3, XLSX file, 0.1 MB.
SUPPLEMENTAL FILE 4, XLSX file, 0.1 MB.
SUPPLEMENTAL FILE 5, XLSX file, 0.1 MB.

ACKNOWLEDGMENTS

REFERENCES

1. Balasuriya U, MacLachlan NJ. 2013. Equine viral arteritis, p 169–181. *In* Sellon DC, Long MT (ed), Equine infectious diseases, 2nd ed. Saunders, St. Louis, MO.
2. Balasuriya UB, Go YY, MacLachlan NJ. 2013. Equine arteritis virus. Vet Microbiol 167:93–122. https://doi.org/10.1016/j.vetmic.2013.06.015.
3. Balasuriya UBR, Carossino M, Timoney PJ. 10 November 2016. Equine viral arteritis: a respiratory and reproductive disease of significant economic importance to the equine industry. Equine Vet Educ https://doi.org/10.1111/eve.12672.
4. Timoney PJ. 2000. The increasing significance of international trade in equids and its influence on the spread of infectious diseases. Ann N Y Acad Sci 916:55–60. https://doi.org/10.1111/j.1749-6632.2000.tb05274.x.
5. Timoney PJ. 2000. Factors influencing the international spread of equine diseases. Vet Clin North Am Equine Pract 16:537–551. https://doi.org/10.1016/S0749-0739(17)30094-9.
6. Timoney PJ, McCollum WH. 1988. Equine viral arteritis: epidemiology and control. J Equine Vet Sci 8:54–59. https://doi.org/10.1016/S0737-0806(88)80112-6.
7. Timoney PJ, McCollum WH. 1993. Equine viral arteritis. Vet Clin North Am Equine Pract 9:295–309. https://doi.org/10.1016/S0749-0739(17)30397-8.
8. Cavanagh D. 1997. Nidovirales: a new order comprising Coronaviridae and Arteriviridae. Arch Virol 142:629–633.
9. Timoney PJ, McCollum WH. 2000. Equine viral arteritis: further characterization of the carrier state in stallions. J Reprod Fertil Suppl 56:3–11.
10. Reference deleted.
11. Timoney PJ, McCollum WH, Murphy TW, Roberts AW, Willard JG, Carswell GD. 1987. The carrier state in equine arteritis virus infection in the stallion with specific emphasis on the venereal mode of virus transmission. J Reprod Fertil Suppl 35:95–102.
12. Balasuriya U. 2014. Equine viral arteritis. Vet Clin North Am Equine Pract 30:543–560. https://doi.org/10.1016/j.cveq.2014.08.011.
13. Balasuriya UB, Snijder EJ, Heidner HW, Zhang J, Zevenhoven-Dobbe JC, Boone JD, McCollum WH, Timoney PJ, MacLachlan NJ. 2007. Development and characterization of an infectious cDNA clone of the virulent Bucyrus strain of equine arteritis virus. J Gen Virol 88:918–924. https://doi.org/10.1099/vir.0.82415-0.
14. Balasuriya UB, Snijder EJ, van Dinten LC, Heidner HW, Wilson WD, Hedges JF, Hullinger PJ, MacLachlan NJ. 1999. Equine arteritis virus derived from an infectious cDNA clone is attenuated and genetically stable in infected stallions. Virology 260:201–208. https://doi.org/10.1006/viro.1999.9817.
15. Go YY, Cook RF, Fulgencio JQ, Campos JR, Henney P, Timoney PJ, Horohov DW, Balasuriya UB. 2012. Assessment of correlation between in vitro CD3+ T cell susceptibility to EAV infection and clinical outcome following experimental infection. Vet Microbiol 157:220–225. https://doi.org/10.1016/j.vetmic.2011.11.031.
16. MacLachlan NJ, Balasuriya UB, Rossitto PV, Hullinger PA, Patton JF, Wilson WD. 1996. Fatal experimental equine arteritis virus infection of a pregnant mare: immunohistochemical staining of viral antigens. J Vet Diagn Invest 8:367–374. https://doi.org/10.1177/104063879600800316.
17. McCollum WH, Timoney PJ, Tengelsen LA. 1995. Clinical, virological and serological responses of donkeys to intranasal inoculation with the KY-84 strain of equine arteritis virus. J Comp Pathol 112:207–211. https://doi.org/10.1016/S0021-9975(05)80062-3.

18. Vairo S, Vandekerckhove A, Steukers L, Glorieux S, Van den Broeck W, Nauwynck H. 2012. Clinical and virological outcome of an infection with the Belgian equine arteritis virus strain 08P178. Vet Microbiol 157:333–344. https://doi.org/10.1016/j.vetmic.2012.01.014.
19. Campos JR, Breheny P, Araujo RR, Troedsson MH, Squires EL, Timoney PJ, Balasuriya UB. 2014. Semen quality of stallions challenged with the Kentucky 84 strain of equine arteritis virus. Theriogenology 82:1068–1079. https://doi.org/10.1016/j.theriogenology.2014.07.004.
20. Vaala WE, Hamir AN, Dubovi EJ, Timoney PJ, Ruiz B. 1992. Fatal, congenitally acquired infection with equine arteritis virus in a neonatal thoroughbred. Equine Vet J 24:155–158. https://doi.org/10.1111/j.2042-3306.1992.tb02803.x.
21. Balasuriya UBR, Sarkar S, Carossino M, Go YY, Chelvarajan L, Cook RF, Loynachan AT, Timoney PJ, Bailey E. 2016. Host factors that contribute to equine arteritis virus persistence in the stallion: an update. J Equine Vet Sci 43:S11–S17. https://doi.org/10.1016/j.jevs.2016.05.017.
22. Reference deleted.
23. Timoney PJ, McCollum WH, Roberts AW, Murphy TW. 1986. Demonstration of the carrier state in naturally acquired equine arteritis virus infection in the stallion. Res Vet Sci 41:279–280.
24. Reference deleted.
25. McCollum WH, Little TV, Timoney PJ, Swerczek TW. 1994. Resistance of castrated male horses to attempted establishment of the carrier state with equine arteritis virus. J Comp Pathol 111:383–388. https://doi.org/10.1016/S0021-9975(05)80096-9.
26. Carossino M, Loynachan AT, Canisso IF, Campos JR, Nam B, Go YY, Squires EL, Troedsson MHT, Cook RF, Swerczek T, Del Piero F, Bailey E, Timoney PJ, Balasuriya UBR. 2017. Equine arteritis virus has specific tropism for stromal cells and CD8+ T and CD21+ B lymphocytes but not glandular epithelium at the primary site of persistent infection in the stallion reproductive tract. J Virol 91:e00418-17. https://doi.org/10.1128/JVI.00418-17.
27. Carossino M, Wagner B, Loynachan AT, Cook RF, Canisso IF, Chelvarajan L, Edwards CL, Nam B, Timoney JF, Timoney PJ, Balasuriya UBR. 2017. Equine arteritis virus elicits a mucosal antibody response in the reproductive tract of persistently infected stallions. Clin Vaccine Immunol 24:e00215-17. https://doi.org/10.1128/CVI.00215-17.
28. Balasuriya UB, Carossino M. 2017. Reproductive effects of arteriviruses: equine arteritis virus and porcine reproductive and respiratory syndrome virus infections. Curr Opin Virol 27:57–70. https://doi.org/10.1016/j.coviro.2017.11.005.
29. Go YY, Bailey E, Cook DG, Coleman SJ, Macleod JN, Chen KC, Timoney PJ, Balasuriya UB. 2011. Genome-wide association study among four horse breeds identifies a common haplotype associated with in vitro CD3+ T cell susceptibility/resistance to equine arteritis virus infection. J Virol 85:13174–13184. https://doi.org/10.1128/JVI.06068-11.
30. Go YY, Bailey E, Timoney PJ, Shuck KM, Balasuriya UB. 2012. Evidence that in vitro susceptibility of CD3+ T lymphocytes to equine arteritis virus infection reflects genetic predisposition of naturally infected stallions to become carriers of the virus. J Virol 86:12407–12410. https://doi.org/10.1128/JVI.01698-12.
31. Sarkar S, Bailey E, Go YY, Cook RF, Kalbfleisch T, Eberth J, Chelvarajan RL, Shuck KM, Artiushin S, Timoney PJ, Balasuriya UB. 2016. Allelic variation in CXCL16 determines CD3+ T lymphocyte susceptibility to

equine arteritis virus infection and establishment of long-term carrier state in the stallion. PLoS Genet 12:e1006467. https://doi.org/10.1371/journal.pgen.1006467.

32. Jasko DJ. 1992. Evaluation of stallion semen. Vet Clin North Am Equine Pract 8:129–148. https://doi.org/10.1016/S0749-0739(17)30471-6.

33. Aumüller G, Seitz J. 1990. Protein secretion and secretory processes in male accessory sex glands. Int Rev Cytol 121:127–231. https://doi.org/10.1016/S0074-7696(08)60660-9.

34. Vojtech L, Woo S, Hughes S, Levy C, Ballweber L, Sauteraud RP, Strobl J, Westerberg K, Gottardo R, Tewari M, Hladik F. 2014. Exosomes in human semen carry a distinctive repertoire of small non-coding RNAs with potential regulatory functions. Nucleic Acids Res 42:7290–7304. https://doi.org/10.1093/nar/gku347.

35. Owen DH, Katz DF. 2005. A review of the physical and chemical properties of human semen and the formulation of a semen simulant. J Androl 26:459–469. https://doi.org/10.2164/jandrol.04104.

36. Rodríguez-Martínez H, Kvist U, Saravia F, Wallgren M, Johannisson A, Sanz L, Pena FJ, Martinez EA, Roca J, Vazquez JM, Calvete JJ. 2009. The physiological roles of the boar ejaculate. Soc Reprod Fertil Suppl 66:1–21.

37. Juyena NS, Stelletta C. 2012. Seminal plasma: an essential attribute to spermatozoa. J Androl 33:536–551. https://doi.org/10.2164/jandrol.110.012583.

38. Larson BL, Salisbury GW. 1954. The proteins of bovine seminal plasma. I. Preliminary and electrophoretic studies. J Biol Chem 206:741–749.

39. Kareskoski M, Katila T. 2008. Components of stallion seminal plasma and the effects of seminal plasma on sperm longevity. Anim Reprod Sci 107:249–256. https://doi.org/10.1016/j.anireprosci.2008.04.013.

40. Caballero I, Parrilla I, Alminana C, del Olmo D, Roca J, Martinez EA, Vazquez JM. 2012. Seminal plasma proteins as modulators of the sperm function and their application in sperm biotechnologies. Reprod Domest Anim 47(Suppl 3):S12–S21. https://doi.org/10.1111/j.1439-0531.2012.02028.x.

41. Aalberts M, Stout TA, Stoorvogel W. 2014. Prostasomes: extracellular vesicles from the prostate. Reproduction 147:R1–R14. https://doi.org/10.1530/REP-13-0358.

42. Lazarevic M, Skibinski G, Kelly RW, James K. 1995. Immunomodulatory effects of extracellular secretory vesicles isolated from bovine semen. Vet Immunol Immunopathol 44:237–250. https://doi.org/10.1016/0165-2427(94)05320-R.

43. Madison MN, Roller RJ, Okeoma CM. 2014. Human semen contains exosomes with potent anti-HIV-1 activity. Retrovirology 11:102. https://doi.org/10.1186/s12977-014-0102-z.

44. Piehl LL, Fischman ML, Hellman U, Cisale H, Miranda PV. 2013. Boar seminal plasma exosomes: effect on sperm function and protein identification by sequencing. Theriogenology 79:1071–1082. https://doi.org/10.1016/j.theriogenology.2013.01.028.

45. Poliakov A, Spilman M, Dokland T, Amling CL, Mobley JA. 2009. Structural heterogeneity and protein composition of exosome-like vesicles (prostasomes) in human semen. Prostate 69:159–167. https://doi.org/10.1002/pros.20860.

46. Arienti G, Carlini E, De Cosmo AM, Di Profio P, Palmerini CA. 1998. Prostasome-like particles in stallion semen. Biol Reprod 59:309–313. https://doi.org/10.1095/biolreprod59.2.309.

47. Colombo M, Raposo G, Thery C. 2014. Biogenesis, secretion, and intercellular interactions of exosomes and other extracellular vesicles. Annu Rev Cell Dev Biol 30:255–289. https://doi.org/10.1146/annurev-cellbio-101512-122326.

48. Kelly RW, Holland P, Skibinski G, Harrison C, McMillan L, Hargreave T, James K. 1991. Extracellular organelles (prostasomes) are immunosuppressive components of human semen. Clin Exp Immunol 86:550–556. https://doi.org/10.1111/j.1365-2249.1991.tb02968.x.

49. Robertson SA, Guerin LR, Bromfield JJ, Branson KM, Ahlstrom AC, Care AS. 2009. Seminal fluid drives expansion of the CD4+CD25+ T regulatory cell pool and induces tolerance to paternal alloantigens in mice. Biol Reprod 80:1036–1045. https://doi.org/10.1095/biolreprod.108.074658.

50. Madison MN, Okeoma CM. 2015. Exosomes: implications in HIV-1 pathogenesis. Viruses 7:4093–4118. https://doi.org/10.3390/v7072810.

51. Valadi H, Ekstrom K, Bossios A, Sjostrand M, Lee JJ, Lotvall JO. 2007. Exosome-mediated transfer of mRNAs and microRNAs is a novel mechanism of genetic exchange between cells. Nat Cell Biol 9:654–659. https://doi.org/10.1038/ncb1596.

52. Bartel DP. 2004. MicroRNAs: genomics, biogenesis, mechanism, and function. Cell 116:281–297. https://doi.org/10.1016/S0092-8674(04)00045-5.

53. Fowler L, Saksena NK. 2013. Micro-RNA: new players in HIV-pathogenesis, diagnosis, prognosis and antiviral therapy. AIDS Rev 15:3–14.

54. Verma P, Pandey RK, Prajapati P, Prajapati VK. 2016. Circulating microRNAs: potential and emerging biomarkers for diagnosis of human infectious diseases. Front Microbiol 7:1274. https://doi.org/10.3389/fmicb.2016.01274.

55. Fiorino S, Bacchi-Reggiani ML, Visani M, Acquaviva G, Fornelli A, Masetti M, Tura A, Grizzi F, Zanello M, Mastrangelo L, Lombardi R, Di Tommaso L, Bondi A, Sabbatani S, Domanico A, Fabbri C, Leandri P, Pession A, Jovine E, de Biase D. 2016. MicroRNAs as possible biomarkers for diagnosis and prognosis of hepatitis B- and C-related-hepatocellular-carcinoma. World J Gastroenterol 22:3907–3936. https://doi.org/10.3748/wjg.v22.i15.3907.

56. Wang J, Chen J, Sen S. 2016. MicroRNA as biomarkers and diagnostics. J Cell Physiol 231:25–30. https://doi.org/10.1002/jcp.25056.

57. Paziewska A, Mikula M, Dabrowska M, Kulecka M, Goryca K, Antoniewicz A, Dobruch J, Borowka A, Rutkowski P, Ostrowski J. 11 December 2017. Candidate diagnostic miRNAs that can detect cancer in prostate biopsy. Prostate https://doi.org/10.1002/pros.23427.

58. He Y, Deng F, Yang S, Wang D, Chen X, Zhong S, Zhao J, Tang J. 2017. Exosomal microRNA: a novel biomarker for breast cancer. Biomark Med https://doi.org/10.2217/bmm-2017-0305.

59. Kim MC, Lee SW, Ryu DY, Cui FJ, Bhak J, Kim Y. 2014. Identification and characterization of microRNAs in normal equine tissues by next generation sequencing. PLoS One 9:e93662. https://doi.org/10.1371/journal.pone.0093662.

60. Desjardin C, Vaiman A, Mata X, Legendre R, Laubier J, Kennedy SP, Laloe D, Barrey E, Jacques C, Cribiu EP, Schibler L. 2014. Next-generation sequencing identifies equine cartilage and subchondral bone miRNAs and suggests their involvement in osteochondrosis physiopathology. BMC Genomics 15:798. https://doi.org/10.1186/1471-2164-15-798.

61. da Silveira JC, Veeramachaneni DN, Winger QA, Carnevale EM, Bouma GJ. 2012. Cell-secreted vesicles in equine ovarian follicular fluid contain miRNAs and proteins: a possible new form of cell communication within the ovarian follicle. Biol Reprod 86:71. https://doi.org/10.1095/biolreprod.111.093252.

62. da Silveira JC, Carnevale EM, Winger QA, Bouma GJ. 2014. Regulation of ACVR1 and ID2 by cell-secreted exosomes during follicle maturation in the mare. Reprod Biol Endocrinol 12:44. https://doi.org/10.1186/1477-7827-12-44.

63. Rout ED, Webb TL, Laurence HM, Long L, Olver CS. 2015. Transferrin receptor expression in serum exosomes as a marker of regenerative anaemia in the horse. Equine Vet J 47:101–106. https://doi.org/10.1111/evj.12235.

64. Aalberts M, Sostaric E, Wubbolts R, Wauben MW, Nolte-'t Hoen EN, Gadella BM, Stout TA, Stoorvogel W. 2013. Spermatozoa recruit prostasomes in response to capacitation induction. Biochim Biophys Acta 1834:2326–2335. https://doi.org/10.1016/j.bbapap.2012.08.008.

65. Kelly RW. 1995. Immunosuppressive mechanisms in semen: implications for contraception. Hum Reprod 10:1686–1693. https://doi.org/10.1093/oxfordjournals.humrep.a136156.

66. Sullivan R, Saez F. 2013. Epididymosomes, prostasomes, and liposomes: their roles in mammalian male reproductive physiology. Reproduction 146:R21–R35. https://doi.org/10.1530/REP-13-0058.

67. Tarazona R, Delgado E, Guarnizo MC, Roncero RG, Morgado S, Sanchez-Correa B, Gordillo JJ, Dejulian J, Casado JG. 2011. Human prostasomes express CD48 and interfere with NK cell function. Immunobiology 216:41–46. https://doi.org/10.1016/j.imbio.2010.03.002.

68. Skibinski G, Kelly RW, Harkiss D, James K. 1992. Immunosuppression by human seminal plasma—extracellular organelles (prostasomes) modulate activity of phagocytic cells. Am J Reprod Immunol 28:97–103. https://doi.org/10.1111/j.1600-0897.1992.tb00767.x.

69. Carissimi C, Carucci N, Colombo T, Piconese S, Azzalin G, Cipolletta E, Citarella F, Barnaba V, Macino G, Fulci V. 2014. miR-21 is a negative modulator of T-cell activation. Biochimie 107(Part B):319–326.

70. Tsukerman P, Stern-Ginossar N, Gur C, Glasner A, Nachmani D, Bauman Y, Yamin R, Vitenshtein A, Stanietsky N, Bar-Mag T, Lankry D, Mandelboim O. 2012. MiR-10b downregulates the stress-induced cell surface molecule MICB, a critical ligand for cancer cell recognition by natural killer cells. Cancer Res 72:5463–5472. https://doi.org/10.1158/0008-5472.CAN-11-2671.

71. Swaminathan S, Suzuki K, Seddiki N, Kaplan W, Cowley MJ, Hood CL,

Clancy JL, Murray DD, Mendez C, Gelgor L, Anderson B, Roth N, Cooper DA, Kelleher AD. 2012. Differential regulation of the Let-7 family of microRNAs in CD4+ T cells alters IL-10 expression. J Immunol 188:6238–6246. https://doi.org/10.4049/jimmunol.1101196.

72. Wells AC, Daniels KA, Angelou CC, Fagerberg E, Burnside AS, Markstein M, Alfandari D, Welsh RM, Pobezinskaya EL, Pobezinsky LA. 2017. Modulation of let-7 miRNAs controls the differentiation of effector CD8 T cells. Elife 6:e26398. https://doi.org/10.7554/eLife.26398.

73. Kumar M, Sahu SK, Kumar R, Subuddhi A, Maji RK, Jana K, Gupta P, Raffetseder J, Lerm M, Ghosh Z, van Loo G, Beyaert R, Gupta UD, Kundu M, Basu J. 2015. MicroRNA let-7 modulates the immune response to Mycobacterium tuberculosis infection via control of A20, an inhibitor of the NF-kappaB pathway. Cell Host Microbe 17:345–356. https://doi.org/10.1016/j.chom.2015.01.007.

74. Podshivalova K, Salomon DR. 2013. MicroRNA regulation of T-lymphocyte immunity: modulation of molecular networks responsible for T-cell activation, differentiation, and development. Crit Rev Immunol 33:435–476. https://doi.org/10.1615/CritRevImmunol.2013006858.

75. Lee S, Hwang S, Yu HJ, Oh D, Choi YJ, Kim MC, Kim Y, Ryu DY. 2016. Expression of microRNAs in horse plasma and their characteristic nucleotide composition. PLoS One 11:e0146374. https://doi.org/10.1371/journal.pone.0146374.

76. Cowled C, Foo CH, Deffrasnes C, Rootes CL, Williams DT, Middleton D, Wang LF, Bean AGD, Stewart CR. 2017. Circulating microRNA profiles of Hendra virus infection in horses. Sci Rep 7:7431. https://doi.org/10.1038/s41598-017-06939-w.

77. Ludwig N, Leidinger P, Becker K, Backes C, Fehlmann T, Pallasch C, Rheinheimer S, Meder B, Stahler C, Meese E, Keller A. 2016. Distribution of miRNA expression across human tissues. Nucleic Acids Res 44:3865–3877. https://doi.org/10.1093/nar/gkw116.

78. Parkinson NJ, Buechner-Maxwell VA, Witonsky SG, Pleasant RS, Werre SR, Ahmed SA. 2017. Characterization of basal and lipopolysaccharide-induced microRNA expression in equine peripheral blood mononuclear cells using next-generation sequencing. PLoS One 12:e0177664. https://doi.org/10.1371/journal.pone.0177664.

79. Dini P, Loux SC, Scoggin KE, Esteller-Vico A, Squires EL, Troedsson MHT, Daels P, Ball BA. 2018. Identification of reference genes for analysis of microRNA expression patterns in equine chorioallantoic membrane and serum. Mol Biotechnol 60:62–73. https://doi.org/10.1007/s12033-017-0047-2.

80. McGivney BA, Griffin ME, Gough KF, McGivney CL, Browne JA, Hill EW, Katz LM. 2017. Evaluation of microRNA expression in plasma and skeletal muscle of thoroughbred racehorses in training. BMC Vet Res 13:347. https://doi.org/10.1186/s12917-017-1277-z.

81. Li M, Fu W, Wo L, Shu X, Liu F, Li C. 2013. miR-128 and its target genes in tumorigenesis and metastasis. Exp Cell Res 319:3059–3064. https://doi.org/10.1016/j.yexcr.2013.07.031.

82. Pacholewska A, Kraft MF, Gerber V, Jagannathan V. 2017. Differential expression of serum microRNAs supports CD4(+) T cell differentiation into Th2/Th17 cells in severe equine asthma. Genes (Basel) 8(12):E383. https://doi.org/10.3390/genes8120383.

83. Nguyen MA, Karunakaran D, Geoffrion M, Cheng HS, Tandoc K, Perisic Matic L, Hedin U, Maegdefessel L, Fish JE, Rayner KJ. 7 September 2017. Extracellular vesicles secreted by atherogenic macrophages transfer microRNA to inhibit cell migration. Arterioscler Thromb Vasc Biol https://doi.org/10.1161/ATVBAHA.117.309795.

84. Geekiyanage H, Galanis E. 2016. MiR-31 and miR-128 regulates poliovirus receptor-related 4 mediated measles virus infectivity in tumors. Mol Oncol 10:1387–1403. https://doi.org/10.1016/j.molonc.2016.07.007.

85. Eletto D, Russo G, Passiatore G, Del Valle L, Giordano A, Khalili K, Gualco E, Peruzzi F. 2008. Inhibition of SNAP25 expression by HIV-1 Tat involves the activity of mir-128a. J Cell Physiol 216:764–770. https://doi.org/10.1002/jcp.21452.

86. Sarkar S, Chelvarajan L, Go YY, Cook F, Artiushin S, Mondal S, Anderson K, Eberth J, Timoney PJ, Kalbfleisch TS, Bailey E, Balasuriya UB. 2016. Equine arteritis virus uses equine CXCL16 as an entry receptor. J Virol 90:3366–3384. https://doi.org/10.1128/JVI.02455-15.

87. Pillai RS. 2005. MicroRNA function: multiple mechanisms for a tiny RNA? RNA 11:1753–1761. https://doi.org/10.1261/rna.2248605.

88. Wang X. 2014. Composition of seed sequence is a major determinant of microRNA targeting patterns. Bioinformatics 30:1377–1383. https://doi.org/10.1093/bioinformatics/btu045.

89. Ravon M, Berrera M, Ebeling M, Certa U. 2012. Single base mismatches in the mRNA target site allow specific seed region-mediated off-target binding of siRNA targeting human coagulation factor 7. RNA Biol 9:87–97. https://doi.org/10.4161/rna.9.1.18121.

90. Brodersen P, Voinnet O. 2009. Revisiting the principles of microRNA target recognition and mode of action. Nat Rev Mol Cell Biol 10:141–148. https://doi.org/10.1038/nrm2619.

91. Hwang I. 2013. Cell-cell communication via extracellular membrane vesicles and its role in the immune response. Mol Cells 36:105–111. https://doi.org/10.1007/s10059-013-0154-2.

92. Raabe CA, Tang TH, Brosius J, Rozhdestvensky TS. 2014. Biases in small RNA deep sequencing data. Nucleic Acids Res 42:1414–1426. https://doi.org/10.1093/nar/gkt1021.

93. National Research Council. 2011. Guide for the care and use of laboratory animals, 8th ed. National Academies Press, Washington, DC.

94. Friedländer MR, Mackowiak SD, Li N, Chen W, Rajewsky N. 2012. miRDeep2 accurately identifies known and hundreds of novel microRNA genes in seven animal clades. Nucleic Acids Res 40:37–52. https://doi.org/10.1093/nar/gkr688.

95. Wade CM, Giulotto E, Sigurdsson S, Zoli M, Gnerre S, Imsland F, Lear TL, Adelson DL, Bailey E, Bellone RR, Blocker H, Distl O, Edgar RC, Garber M, Leeb T, Mauceli E, MacLeod JN, Penedo MC, Raison JM, Sharpe T, Vogel J, Andersson L, Antczak DF, Biagi T, Binns MM, Chowdhary BP, Coleman SJ, Della Valle G, Fryc S, Guerin G, Hasegawa T, Hill EW, Jurka J, Kiialainen A, Lindgren G, Liu J, Magnani E, Mickelson JR, Murray J, Nergadze SG, Onofrio R, Pedroni S, Piras MF, Raudsepp T, Rocchi M, Roed KH, Ryder OA, Searle S, Skow L, Swinburne JE, Syvänen AC, Tozaki T, Valberg SJ, Vaudin M, White JR, Zody MC, Broad Institute Genome Sequencing Platform, Broad Institute Whole Genome Assembly Team, Lander ES, Lindblad-Toh K. 2009. Genome sequence, comparative analysis, and population genetics of the domestic horse. Science 326:865–867. https://doi.org/10.1126/science.1178158.

96. Kozomara A, Griffiths-Jones S. 2011. miRBase: integrating microRNA annotation and deep-sequencing data. Nucleic Acids Res 39:D152–D157. https://doi.org/10.1093/nar/gkq1027.

97. Kozomara A, Griffiths-Jones S. 2014. miRBase: annotating high confidence microRNAs using deep sequencing data. Nucleic Acids Res 42:D68–D73. https://doi.org/10.1093/nar/gkt1181.

98. Chan PP, Lowe TM. 2009. GtRNAdb: a database of transfer RNA genes detected in genomic sequence. Nucleic Acids Res 37:D93–D97. https://doi.org/10.1093/nar/gkn787.

99. Wong N, Wang X. 2015. miRDB: an online resource for microRNA target prediction and functional annotations. Nucleic Acids Res 43:D146–D152. https://doi.org/10.1093/nar/gku1104.

100. Vlachos IS, Paraskevopoulou MD, Karagkouni D, Georgakilas G, Vergoulis T, Kanellos I, Anastasopoulos IL, Maniou S, Karathanou K, Kalfakakou D, Fevgas A, Dalamagas T, Hatzigeorgiou AG. 2015. DIANA-TarBase v7.0: indexing more than half a million experimentally supported miRNA:mRNA interactions. Nucleic Acids Res 43:D153–D159. https://doi.org/10.1093/nar/gku1215.

101. Chou CH, Chang NW, Shrestha S, Hsu SD, Lin YL, Lee WH, Yang CD, Hong HC, Wei TY, Tu SJ, Tsai TR, Ho SY, Jian TY, Wu HY, Chen PR, Lin NC, Huang HT, Yang TL, Pai CY, Tai CS, Chen WL, Huang CY, Liu CC, Weng SL, Liao KW, Hsu WL, Huang HD. 2016. miRTarBase 2016: updates to the experimentally validated miRNA-target interactions database. Nucleic Acids Res 44:D239–D247. https://doi.org/10.1093/nar/gkv1258.

102. Agarwal V, Bell GW, Nam JW, Bartel DP. 2015. Predicting effective microRNA target sites in mammalian mRNAs. Elife 4:e05005. https://doi.org/10.7554/eLife.05005.

103. Mann M, Wright PR, Backofen R. 2017. IntaRNA 2.0: enhanced and customizable prediction of RNA-RNA interactions. Nucleic Acids Res 45:W435–W439. https://doi.org/10.1093/nar/gkx279.

104. Rehmsmeier M, Steffen P, Hochsmann M, Giegerich R. 2004. Fast and effective prediction of microRNA/target duplexes. RNA 10:1507–1517. https://doi.org/10.1261/rna.5248604.

105. Ghoshal A, Shankar R, Bagchi S, Grama A, Chaterji S. 2015. MicroRNA target prediction using thermodynamic and sequence curves. BMC Genomics 16:999. https://doi.org/10.1186/s12864-015-1933-2.

106. Huang da W, Sherman BT, Lempicki RA. 2009. Systematic and integrative analysis of large gene lists using DAVID bioinformatics resources. Nat Protoc 4:44–57. https://doi.org/10.1038/nprot.2008.211.

107. Huang da W, Sherman BT, Lempicki RA. 2009. Bioinformatics enrichment tools: paths toward the comprehensive functional analysis of large gene lists. Nucleic Acids Res 37:1–13. https://doi.org/10.1093/nar/gkn923.

108. Mi H, Huang X, Muruganujan A, Tang H, Mills C, Kang D, Thomas PD.

2017. PANTHER version 11: expanded annotation data from gene ontology and reactome pathways, and data analysis tool enhancements. Nucleic Acids Res 45:D183–D189. https://doi.org/10.1093/nar/gkw1138.

109. Busk PK. 2014. A tool for design of primers for microRNA-specific quantitative RT-qPCR. BMC Bioinformatics 15:29. https://doi.org/10.1186/1471-2105-15-29.

110. Cirera S, Busk PK. 2014. Quantification of miRNAs by a simple and specific qPCR method. Methods Mol Biol 1182:73–81. https://doi.org/10.1007/978-1-4939-1062-5_7.

111. Ruijter JM, Ramakers C, Hoogaars WM, Karlen Y, Bakker O, van den Hoff MJ, Moorman AF. 2009. Amplification efficiency: linking baseline and bias in the analysis of quantitative PCR data. Nucleic Acids Res 37:e45. https://doi.org/10.1093/nar/gkp045.

112. Andersen CL, Jensen JL, Orntoft TF. 2004. Normalization of real-time quantitative reverse transcription-PCR data: a model-based variance estimation approach to identify genes suited for normalization, applied to bladder and colon cancer data sets. Cancer Res 64:5245–5250. https://doi.org/10.1158/0008-5472.CAN-04-0496.

113. Carossino M, Loynachan AT, James MacLachlan N, Drew C, Shuck KM, Timoney PJ, Del Piero F, Balasuriya UB. 19 August 2016. Detection of equine arteritis virus by two chromogenic RNA in situ hybridization assays (conventional and RNAscope(R)) and assessment of their performance in tissues from aborted equine fetuses. Arch Virol https://doi.org/10.1007/s00705-016-3014-5.

114. Schmittgen TD, Livak KJ. 2008. Analyzing real-time PCR data by the comparative C(T) method. Nat Protoc 3:1101–1108. https://doi.org/10.1038/nprot.2008.73.